Density Functional Theory Calculation of Barrier to Ligand Binding in Myoglobin

Benjamin H. McMahon, Branko P. Stojković,
P.J. Hay, R.L. Martin, A. García

Center for Nonlinear Studies and Theoretical Division
Los Alamos National Laboratory
Los Alamos, NM 87545

May 1999

Abstract

We present a microscopic model of carbon monoxide (CO) binding to myoglobin from the heme pocket which reproduces the experimentally observed enthalpy barrier of 12 kJ/mol and Arrhenius pre-exponential factor of 10^9 s^{-1}. *Ab-initio* calculations of CO interacting with a model heme-imidazole group were performed with a fully quantum mechanical Hartree-Fock/density functional theory hybrid method. The energy of one thousand heme-CO structures with varied CO positions and orientations, iron-heme plane distances, and spin states were calculated and fit to a model potential. This potential includes a bonding interaction in both the high and low spin state, electrostatic, and anisotropic Lennard-Jones-like interactions. When combined with protein-CO interactions and heme motions obtained from established molecular dynamics literature, it is possible to calculate the energy required for the CO to reach the spin crossing from the heme pocket. We find that the classical, adiabatic transition state involves 6 kJ/mol given to the CO, 2.5 kJ/mol to move the iron relative to the heme plane N_{pyr}, and 4 kJ/mol to move N_ϵ of H64 and C_γ of V68 relative to the heme group. The requirement that these motions be synchronized reduces the Arrhenius pre-exponential by a factor of 125 from the 10^{12} s^{-1} obtained from CO motion across the heme pocket. Conformational relaxation is characterized by comparing the X-ray structures of photoproduct and deoxy myoglobin. We illustrate a quantitative method for calculating the effect of tertiary structural changes or mutagenesis on the CO rebinding barrier. The estimated dependence of the enthalpy barrier on changes in protein structure agrees well with the observed width of the enthalpy distribution and B-factors from x-ray crystallography. Changes in the electrostatic field produced by the heme upon CO binding and as the iron moves into the heme plane are characterized and effects of external charges are discussed.

1   Introduction

Calculation of protein function from its structure has been a long-time goal of molecular biology. The interaction of small ligands such as CO, O_2 and NO with heme proteins has been studied extensively, both because of their physiological importance and their experimental accessibility. Although extensive physiological [91, 92, 74], structural [50, 18, 78, 90, 83], dynamic [69, 22, 16, 86], and functional [6, 67, 44, 10] studies of myoglobin make it a prime example for testing the applicability of reaction rate theories [36] to proteins [28, 94], a microscopic description of the ligand binding step does not yet exist.

Atomic resolution coordinates of all heavy atoms in myoglobin have been determined by Schlichting et al. [78], for both bound and photo-dissociated CO-myoglobin at 15 K. We present a comparison of these structures in Figure 1, with protons added by AMBER. The largest changes in myoglobin structure between the CO bound and low temperature photoproduct states [78] are the motion of the CO and the iron atom, but numerous smaller changes also occur. We combine our heme-CO model potential with standard potentials used previously in MD simulations in order to calculate the barrier to CO recombining from this configuration.

Additional structural information on the CO binding site comes from optical [25] Raman [70], infra-red [4], Mössbauer [69], NMR [61, 12], EPR [39] and XAFS [79] spectroscopies, as well as X-ray [50] and neutron [18] crystallography, mutagenesis [83] and studies of model heme compounds [19, 81, 8]. Dynamics has been characterized by temperature dependent Mössbauer spectroscopy [69, 66], inelastic neutron scattering [22] and molecular dynamics simulations [84, 86]. Estimates of conformational disorder is taken from X-ray crystallography [27, 29, 90].

The recombination kinetics have been extensively characterized. The relevant information can be found in Austin et al. [6], and is summarized in Figure 1. Between 50 and 180 K, the CO recombination, $N(t)$, is described by a static distribution of enthalpy barriers, $g(H)$

$$N(t) = \int g(H) \exp(-k(H,T)t)dt, \tag{1}$$

and follows the Arrhenius law with a single pre-exponential factor, A_0:

$$k(H,T) = A_0 \frac{T}{100\ K} \exp\left(-\frac{H}{k_B T}\right), \tag{2}$$

where $A_0 = 10^9\ \mathrm{s}^{-1}$ and $g(H)$ is peaked at 12 kJ/mol and a width of 7 kJ/mol. The substantial width of the distribution is due to a variety of protein conformations trapped as the protein sample is frozen [6]. Multiple flash experiments [6, 71] demonstrate that this distribution is static, rather than dynamic in origin. Austin et al. [6] also noted that the low temperature enthalpy barrier is observed in recombination from the solvent above ~ 250 K, when the probability of escape to the solvent is high, and so a pre-equilibrium exists between D and S. Comparison of the tunneling rate of ^{13}CO and $C^{18}O$ (observable below 30 K) suggests that the binding step occurs as a rotation about the oxygen atom [3].
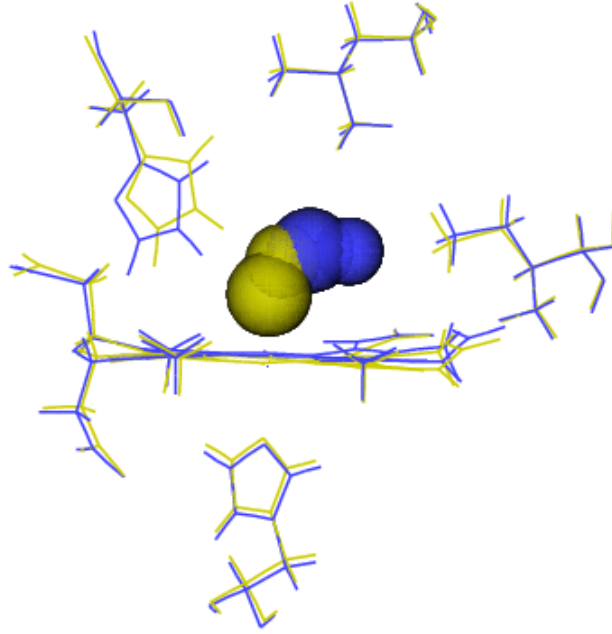
(a)
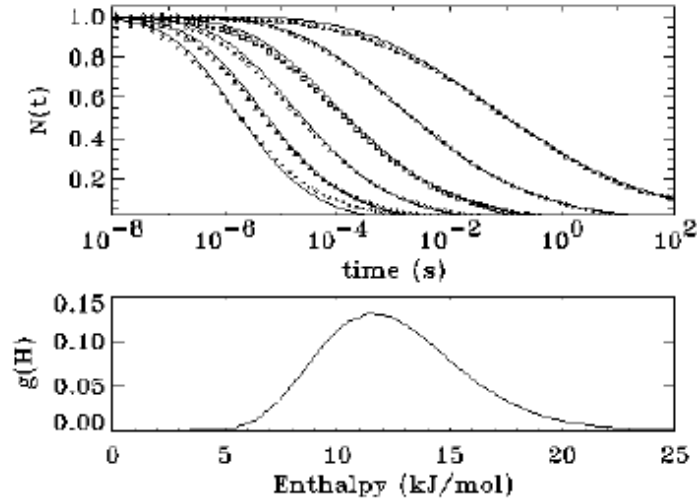
(b), (c)

Figure 1: **(a)** The active site of sperm whale myoglobin in the CO bound state and the 20 K photoproduct state, determined by x-ray diffraction from myoglobin crystals. (Schlichting et al.[78]). The two structures were aligned by the planar atoms of the heme group. **(b)** Kinetics of CO recombination to horse heart myoglobin (solid lines) with fit to enthalpy barrier distribution using a 10^9 s^{-1} preexponential factor, and (13) (dotted lines). **(c)** Distribution of enthalpy barriers from fit shown in **(b)**.

Many simulations of ligand motion in myoglobin have been published [47, 84, 40, 89, 94, 15, 35], and Lennard-Jones and Coulomb interaction parameters have been developed which reproduce a variety of experimentally observed behaviors and *ab-initio* quantum chemical calculations [20, 58]. All have suffered from the lack of a heme–ligand potential which is accurate throughout the active site, includes the non-trivial effects of iron motion relative to the heme plane, and provides both the low spin (S=0) and high spin (S=2) potentials. Another problem is that the longest myoglobin simulation to date has been 1 ns, coincidentally equal to the prefactor in this basic binding step.

Myoglobin data [42] and RC work [60] imply that timescales out to at least microseconds are important. Although Kollman [45] were able to simulate protein motion for a full microsecond, it not at the level of detail necessary to calculate reaction rates. Such calculations require a method of separating the problem of characterizing of protein motions and the effect of these motions on the function of the active site of the protein.

Details of motions at the active site of proteins can be understood using density functional theory calculations, which have been recently reviewed by Barends and Gritsenko [7]. Previous quantum mechanical (QM) calculations of CO stretch frequency [41, 51, 52], spectral properties and electronic structures [33, 43, 25, 17, 24, 23, 56, 88, 75, 76] of heme groups have steadily improved. Recent calculations using the hybrid HF / DFT functional of Becke [11] have quantitatively reproduced Mössbauer and NMR interaction parameters [61] for low spin heme-imidazole-CO, vibrational frequencies of iron(II) porphine [46], and provided reasonable energies for tilting and bending the bound CO [82]. Recent studies of heme-O_2 by Loew et al. [56, 57, 37] have been published. It seems reasonable to expect semi-quantitative agreement between calculation and experiment, even in transition metal systems.

The well characterized structure and function of myoglobin have encouraged many new ideas in reaction rate theory of proteins [10, 2, 28, 36, 85, 68]. This work continues this pattern, providing a quantative link between DFT calculations and experimental measurement on an experimentally accessible system. Such a link will eliminate (or at least provide a method to calculate, *ab-initio*, the phenomenological parameters which have always been necessary when comparing theses theories to experiment.

With a wide variety of enzyme reactions within reach of quantum chemical calculation [59, 21, 37, 53], it is important to examine to what extent protein dynamics influences results in a system (myoglobin) where this is possible. Calculations of comparable difficulty to the present could address the multitude of suggestions of allosteric mechanisms in heme proteins, such as the R to T state transition which allows cooperative binding of oxygen to hemoglobin. It is a necessary first step in understanding the active sites of more complex protein interactions, such as proton pumping in cytochrome c oxidase or peroxidase activity of P-450, as well as the multitude of cases where the structure is known and physiological role is only partially understood.

We present *ab-initio* calculations of the interaction potential between CO and the heme iron atom atom for many different geometric configurations, and both the high (S=2) and low (S=0) spin states. The entire heme group, bound imidazole ligand, and free CO ligand were

included in this QM calculation because the electronic states of all change during binding. Calculated heme properties are presented, including electrostatics and interaction potentials. We fit our results to a model function and explain each component interaction. Inclusion of protein-CO interactions in the simplest possible way allows the effect of vibrations and conformational distributions to be approximated, providing the enthalpy barrier and the preexponential factor of CO recombination to sperm whale myoglobin.

We predict the extent to which the barrier changes as the protein fluctuates, the change in the barrier with protein adaptation to its unligated conformation, and the effect of protonation of H64 or amino acid substitution, all of which we compare to experiment.

2   Materials and Methods

We use the standard Gaussian 94 package and the hybrid density functional theory Hamiltonian of Becke (B3LYP) [11], which yields the spatial distribution of the electronic density and total energy of the system.

The following basis sets were used for all reported results: `6-311+g` for iron, `6-31g` for ligand (CO), and `3-21g` for all other atoms. The basis set was of minimal size so that convergence could be obtained for a wide variety of configurations in a reasonable amount of time. The polarizability was calculated as a function of the iron-heme plane distance for both high and low spin, with the `6-31g**` basis set for all C, N, and H, with no significant changes. No symmetry properties were incorporated into the calculations, and the total electronic spin was restricted to either 0 or 2, essentially all of which resided on the iron atom.

The term *ab-initio* should not be taken too literally, since there is an element of empiricism involved in choosing the hybrid density functional and Gaussian basis set [11, 64] for the calculation. Nevertheless, these choices were made on the basis of previous calculations, and were not treated as parameters.

In each of the calculations we assume a fixed geometry, i.e., we perform only single point calculations. We reach the final convergence gradually: typically, we start with calculations using the Hartree-Fock Hamiltonian and orbitals from an initial guess of linear combinations of atomic orbitals with the `3-21g` basis set. On applying progressively more complex methods and basis sets and eliminating an arbitrary shift of unoccupied orbitals upwards in energy, we reach the final convergence to 1 kJ/mol overall. Occasionally, 'annealing' of the system was needed in the form of iron or ligand motion to reach final convergence. In the high spin state, the initial convergence typically requires about six hours of real time on a four processor Origin 200 SGI workstation. Additional calculations were performed by applying small changes (~ 0.1 Å) to the structure, and required approximately one hour per structure. We have verified that the obtained results do not depend on the initial guess, the initial ligand position, or the details involved in obtaining convergence.

3 Geometry

In order to obtain experimentally relevant results one has to include at least 48 atoms in this calculation. The iron orbitals are strongly hybridized with the proximal histidine and delocalized π-electron system of the heme, so both of these systems must be included. Because the distal pocket is not covalently bonded to the heme, we do not include the rest of the protein in the QM calculation. Instead, we estimate the electrostatics and polarizability of the system, and verify that it behaves in a relatively simple fasion. Out of the 48 atoms used: two are ligand atoms (CO), 37 heme atoms, and 9 are protein atoms, most with fixed coordinates, as listed in Table 1. All 236 electrons were included explicitly.

The protein atom coordinates have been obtained from x-ray studies of model porphyrin compounds and myoglobin. Note that our model heme shown in Figure 2 possesses tetragonal (C_{4v}) symmetry; hence only the coordinates for one quarter of the heme plane are listed

atom	x	y	z	$q(0,0)$	$q(2,0)$	$q(2,0.3)$
Fe	0.0	0.0	0.0	2.22	1.58	1.64
N_ϵ	0.0	0.0	-2.109	-0.50	0.06	-0.42
N_{pyr}	2.075	0.0	0.0	-1.04	-1.07	-1.02
C_α	2.898	1.133	0.0	0.63	0.69	0.69
C_β	4.229	0.700	0.0	-0.30	-0.33	-0.33
C_m	2.465	2.465	0.0	-0.63	-0.62	-0.64
H_β	5.103	1.335	0.0	0.16	0.18	0.17
H_m	3.228	3.228	0.0	0.20	0.18	0.18
C_ϵ	1.071	0.083	-2.880	0.18	-0.03	0.17
$H_{C\epsilon}$	2.079	0.161	-2.531	0.07	0.14	0.07
N_δ	0.711	0.055	-4.202	-0.23	-0.26	-0.23
$H_{N\delta}$	1.355	0.105	-5.004	0.32	0.34	0.32
C_γ	-0.682	-0.053	-4.254	-0.19	-0.12	-0.17
$H_{C\gamma}$	-1.211	-0.094	-5.183	0.18	0.16	0.17
C_δ	-1.104	-0.085	-2.977	0.06	-0.18	0.05
$H_{C\delta}$	-2.096	-0.162	-2.584	0.09	0.16	0.08
C	0.0	0.0	1.800	0.08	0.02	0.02
O	0.0	0.0	2.930	-0.26	-0.02	-0.02
Ring				2.15	2.45	2.36
Core				-2.46	-2.65	-2.84
Im				0.49	0.21	0.47
CO				-0.18	0.00	0.00

Table 1: Atom coordinates (in Å) used in the QM calculation. Only one forth of the atoms with $z = 0$ (heme plane) are listed as all others can be obtained by symmetry. CO coordinates are given for a 'reactant' configuration.
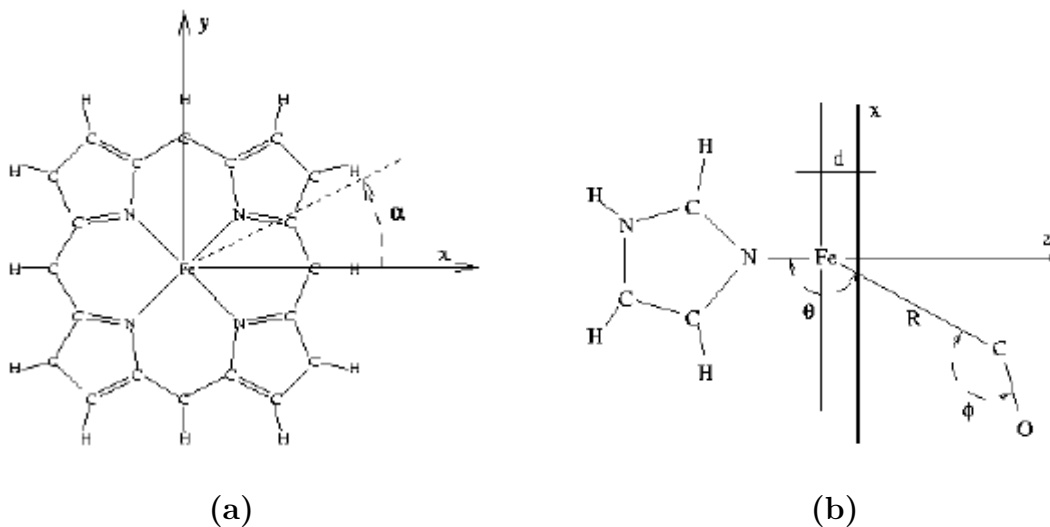
(a)   (b)

Figure 2: Heme-imidazole-CO complex used in the DFT calculation, defining the structure, the parameters R, d, θ, ϕ, and α, which characterize CO binding, and the coordinates x, y, and z, which are used when the effects of additional protein atoms are included. **(a)** Top view, showing all of the atoms in the heme plane. **(b)** Side view, showing the imidazole ring and the CO ligand. The CO is denoted as AB because it is sometimes convenient to define R with respect to the oxygen atom, as we do in several plots. Unless clearly specified otherwise, however, A is the CO carbon and B is the CO oxygen.

(atoms with $z = 0$ in Table 1).

The coordinates varied in order to determine the relevant interactions are defined in Figure 2. Figure 2b shows a cross section of a typical geometric configuration we study: we specify the ligand position by the distance of the C (or O) atom from the Fe atom and a polar angle θ, $\pi/2 < \theta < \pi$, between the z-axis and the line connecting Fe and C atom. Note that $\theta = \pi$ when the carbon atom is directly above Fe when viewed from the symmetry axis of the heme plane (see Figure 2a). The orientation of the ligand is specified by an angle ϕ between line connecting C and O and the line which connects Fe and C and by an angle α between the projection of the C-O bond onto the heme plane and the x-axis, defined as a reflection symmetry line, lying between two nitrogens in the heme plane. We will keep $\alpha \sim 0$ in most of the plots below. Note that $\phi = \pi$ when CO is pointed at the iron atom.

While other coordinates are undoubtedly important, they can be taken into account by applying standard MD parameters, which are derived in part from experiment. For example, the dependence of the iron out of plane distance on the angle of the imidazole ring will appear from Lennard-Jones repulsion. Likewise for heme ruffling. The four coordinates chosen are inherently more complex, and are not adequately treated with standard molecular dynamics force fields.
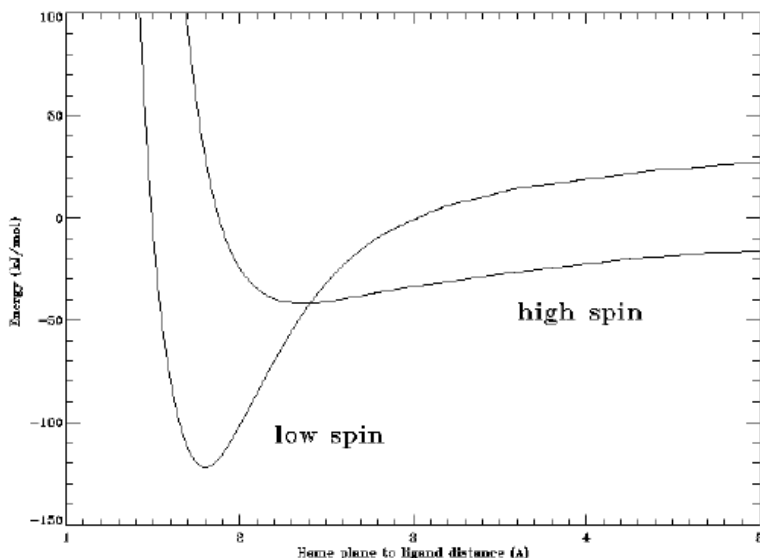
7

Figure 3: Energy of 48 atom system as CO approaches the iron atom along the z-axis with the iron in the heme plane ($V(R)$ for $d = 0, \theta = \phi = 180, \alpha = 0$) for both the high (S=2) and low (S=0) spin states.

4 DFT Results

Figure 3 shows that CO binds to the model heme group in the low spin state with the iron atom in the heme plane. When the CO dissociates, the iron changes to spin 2 and moves out of the heme plane. The binding energy (80 kJ/mol) and equilibrium bond lengths for Fe-CO (1.80 Å) and Fe-heme plane (0.0, 0.25 Å), are in reasonable agreement with experiment [90]. Both the position and energy of the spin crossing change dramatically with d, the iron-heme plane distance.

According to this calculation, CO can bind without an enthalpy barrier if it is allowed to approach the heme iron atom along the heme symmetry axis. The observed enthalpy appears because the protein restricts access to the iron. Consequently, we must parameterize a representative sample of both high and low spin interaction configurations and combine with CO-protein interactions in order to calculate the barrier to recombination.

4.1 High Spin Potential

In Figures 4, 5 and 6 we show the energy of the high spin heme–CO system as a function of the coordinates defined in Figure 2. The result of the QM calculations are shown as symbols and the line is a fit to a model function which is explained in the next section.

A simultaneous fit to all twelve configurations is needed to uniquely separate bonding interactions from Lennard-Jones and electrostatic interactions; fewer configurations results
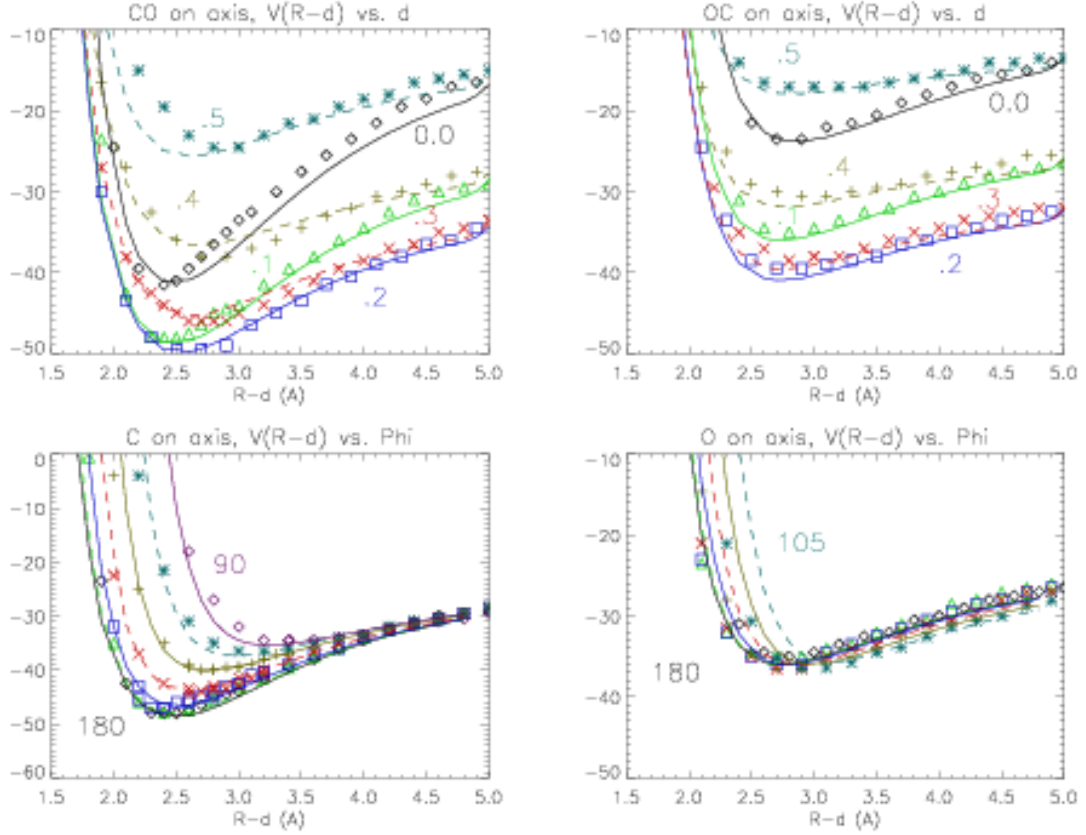
Figure 4: Energy of structures which characterize the high spin bonding interaction. Symbols are energies from DFT calculations and lines show the model function described in text. **Upper left (a)** $V(R)$ at different iron-heme plane distances; d=0, diamonds; 0.1 Å, (triangles); 0.2 Å, squares; 0.3 Å, (x); 0.4 Å, (+); 0.5 Å(*). $\theta = \phi = 180$, α =0. **Lower left (b)** $V(R)$ at different CO orientations; ϕ=180, (diamonds); 165, (triangles); 150, (squares); 135, (x); 120, (+); 105, (*); 90, (diamonds). d=0.1 Å, $\theta = 180$, α=0. **Upper right (c)** Same as **(a)**, except with oxygen atom closest to iron (oxygen is atom A in Figure 2). **Lower right (d)** Same as **(b)**, except with oxygen atom closest to iron (oxygen is atom A in Figure 2).
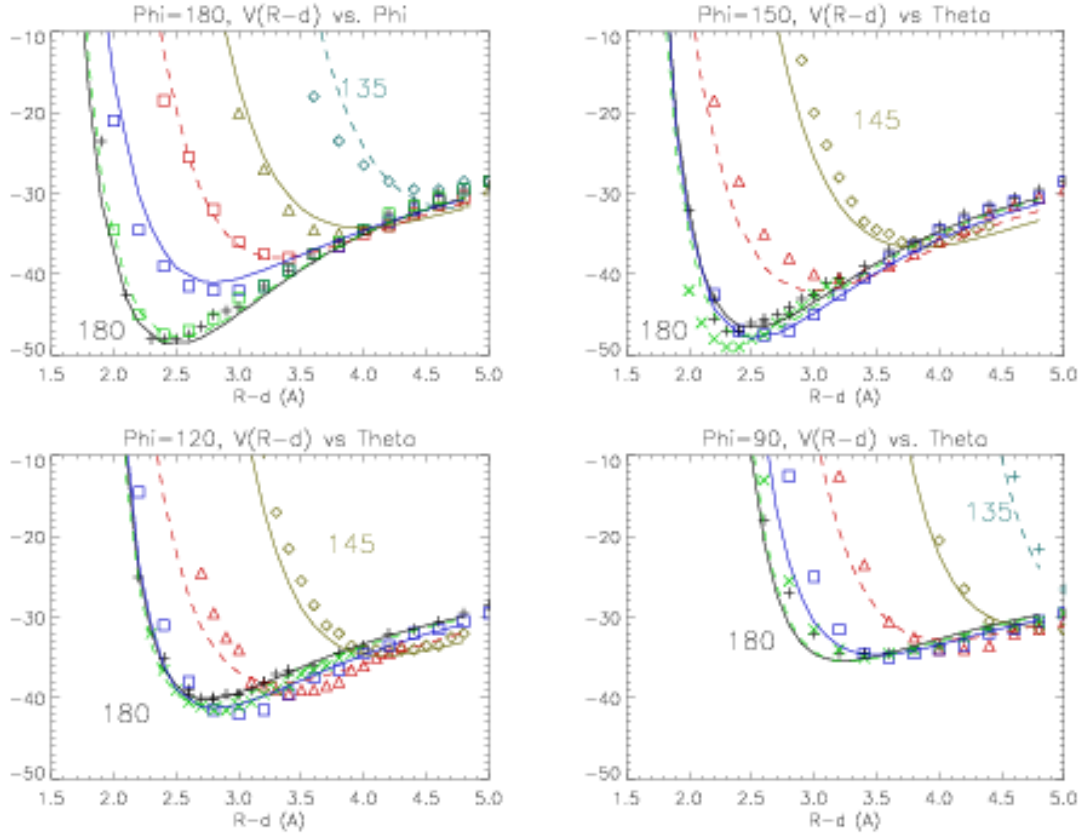
9

Figure 5: Energy of structures which characterize binding by translation. $V(R)$ at different values of θ; θ=180, (diamonds); 175, (triangles); 165 (squares); 155, (x); 145, (+); 135 (*); with d=0.1 Å, α=0 and **(a)** ϕ=180, **(b)** ϕ=150, **(c)** ϕ=120, and **(d)** ϕ=90.
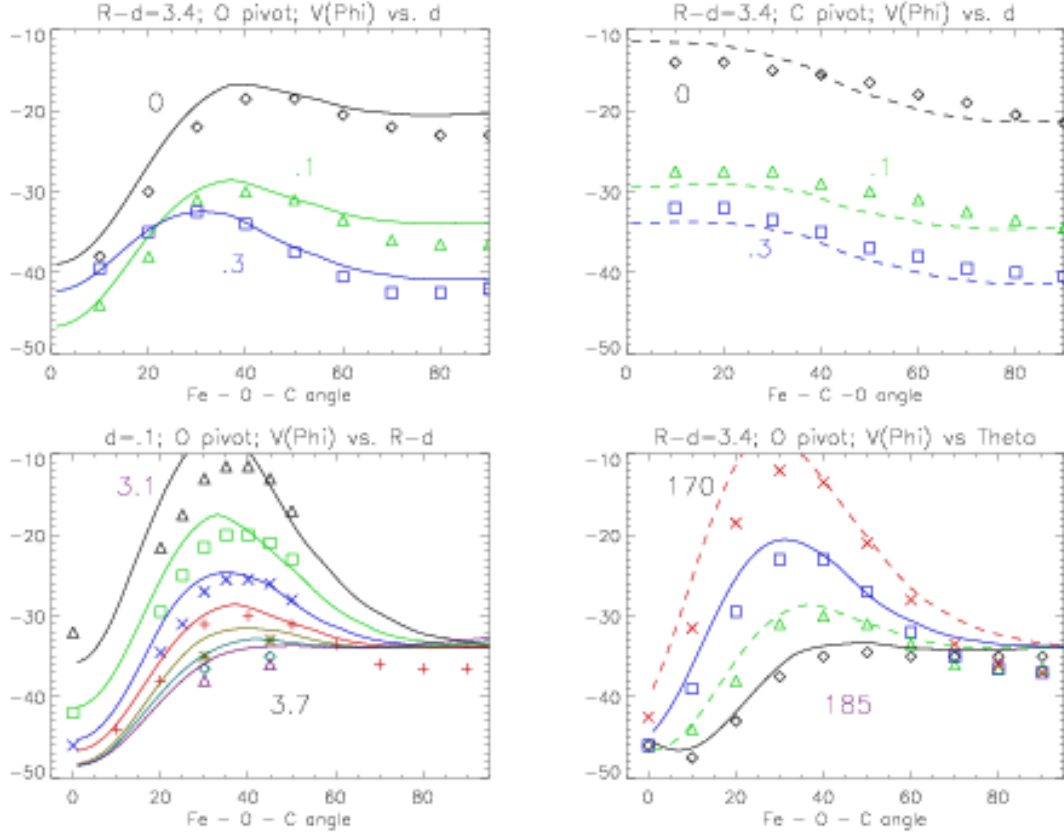
Figure 6: Energy of structures which characterize binding by rotation. **Upper left (a)** $V(\phi)$ for d=0.0 Å, (diamonds); 0.1 Å, (triangles); 0.3 Å, (x); with $\theta = 180, \alpha$=0 and $R-d$=3.4 Å, where O is the pivot (oxygen is A in Figure 2). **Lower left (b)** $V(\phi)$ at different iron-oxygen distances of $R-d$=3.1 Å, (diamonds); 3.2 Å, (triangles); 3.3 Å, (squares); 3.4 Å, (x); 3.5 Å, (+); 3.6 Å, (*); 3.7 Å(diamonds); with d=0.1 Å, θ=180, and α=0. **Upper right (c)** Same as **(a)**, except with carbon atom as pivot. **Lower right (d)** $V(\phi)$ at different x values of the pivot point: θ=185, (diamonds); 180, (triangles); 175, (squares); 170, (x); for d=0.1 Å, $R-d$=3.4 Å, α=0. The 5 degree changes in θ result in a 0.15 Ådisplacement in the x direction of the oxygen atom (which is atom A in Figure 2).

in ambiguity, while more configurations simply adds redundancy or unnecessary complexity. Consequently, we discuss the physical origin of the interactions in the next section, when our model fit function is described. Here we explain the relevance and physical consequences of the *ab-initio* calculations performed.

We have grouped the high spin calculations into three figures, according to which aspect of the heme-CO interaction they show. Figure 4 characterizes the bonding interaction, Figure 5 characterizes binding by translational motion, and Figure 6 characterizes binding by rotation. The calculated effect of external electric fields and rotation of the imidazole ligand are explained in the text, after the model fit function is described.

The calculations in Figure 4 show an attraction of CO to the heme iron atom in the high spin state. It is approximately 15 kJ/mol between the iron and carbon atom and 5 kJ/mol between the iron and oxygen atom. The four panels characterize the iron-heme plane distance and angular (ϕ) dependence of the Fe-C and Fe-O interaction.

Figure 4a shows the change in Fe-C radial binding potential as a function of the iron out of heme plane distance, d. The bond strengthens significantly, narrows, and moves towards the iron as the iron moves into the heme plane. The iron moves 0.1 Å closer to the heme plane when the ligand is present. Similar, but much smaller effects are observed for the Fe-O interaction in Figure 4c.

The medium range (3–5 Å) decay of the radial potential like $r^{-1.8}$ provides a significant attraction (greater than $k_B T$) even 5 Å from the heme plane. The shortest range repulsion is observed by its dependence on d to be hard core repulsion of the iron and carbon, while d-dependence of the bond strength affects the equilibrium iron-ligand distance.

Figure 4b shows the angular (ϕ) dependence of the iron-carbon bonding interaction strength. It is seen to drop to zero strength when $\phi = 90$ degrees. In Figure 4d, we see that the angular (ϕ) dependence of the iron-oxygen interaction is much weaker. Indeed, the strongest Fe-O interaction is for $\phi = 165$, rather than 180 degrees. This atom- specific dependence and the observation that the interaction drops to zero strength but does not become repulsive both suggest that we are observing an orientation dependent bonding interaction, and not the sum of an isotropic attraction and L-J repulsion from the heme nitrogens.

Further separation of the orientation dependent attraction and van der Waals repulsion is made in Figure 5, where we show the potential as a function of both θ and ϕ, attempting to include representative van der Waals interactions between CO and the heme nitrogens and carbons, ranging from Figure 5a, where the side of the carbon runs into the nitrogen to Figure 5d, where the oxygen is the culprit. Calculated configurations fill the entire heme pocket, but were restricted to configurations where the CO carbon is closest to the iron atom. These calculations show how close the CO can get to the heme nitrogen atoms as it scrapes past on its way to the iron atom.

It is easily seen that the bonding interaction disappears for $\phi = 90$ degrees, irrespective of the value of θ, but most of the information in these plots is convoluted by the difficulty of understanding how e.g. the carbon-nitrogen distance depends on θ, ϕ, and $R - d$. Rather than attempting to plot the calculations along lines chosen to show primarily a particular

interaction, we simply cover all possible orientations and positions of the CO 'binding by translation' in Figure 5 and 'binding by rotation' in Figure 6 with these three parameters and then fit the whole group to a model function. We have observed that each L-J parameter of our model fit function significantly affects the fit in at least one of the plots.

The crossing of the curves, seen in Figures 5b and c, cannot be due to radial L-J type interactions, and required us to include an electrostatic heme-CO interaction.

Binding by rotation, Figure 6, involving end-on interactions of the CO with the heme nitrogens, directly shows a barrier to recombination. This is because the interaction of the pivot atom with the rest of the protein will not change as ϕ decreases. Figure 6a, with the oxygen pivot placed on the heme axis, 3.4 Å from the heme plane, approximates a transition state accessible in myoglobin. The barrier appears at an Fe-O-C angle of $\sim$ 35 degrees. Furthermore, Figure 6b and d show that this barrier height depends greatly on the placement of the pivot point, both in distance from the heme plane (Figure 6b) and distance from the heme symmetry axis (Figure 6d). At R_{pivot} of 3.0 Å, the barrier is 35 kJ/mol, while at a 3.6 Å distance, recombination is barrierless. The sensitivity of the energy to 0.1 Å changes in the structure remains in more careful treatments.

The iron-heme plane distance changes the character of the potential considerably, both for oxygen pivot, Figure 6a, and for carbon pivot, Figure 6c. These plots are the most difficult to understand, as nearly every type of interaction changes along the x coordinate (ϕ). In particular, the maximum is located nearly when the CO is closest to the heme nitrogens, as expected if the barrier results from Lennard-Jones repulsion from this atom. The dependence of this barrier on d, however, shows that the bonding interaction plays a significant role.

The d-dependence of the binding by rotation shows that the angular dependence in is the bonding interaction, not L-J. Also, the sharp drop for $\phi < 30$ degrees measures the width of the bond in the x-direction. Compare it to the radial dependence in Figure 4a, remembering that the CO bond length is 1.13 Å.

A point charge of one e placed 5 Å above the heme nitrogens (at the position of His64) had no calculable effect on the shape of the potentials shown here, although a parabolic dependence of the energy on the magnitude of the charge demonstrated that the polarizability of the heme is more important than its dipole moment in interactions of small charges which are near the active site.

4.2   Low-Spin Potential

The radial dependence of the low spin potential is presented in Figure 7a, as a function of d. The bond is much stronger and narrower than in the high spin state and the bond length is shorter. Also, the iron likes to sit closer to the heme plane, and the van der Waals radius is smaller, as expected from inorganic chemist's presentation [34]. The electrostatic contribution to binding is larger, simply because the CO is closer to the iron.

In Figure 7b, we show two angular dependencies. First, the decrease in bond strength which comes from changing ϕ, and second, the increase in L-J (CO-N) energy which comes
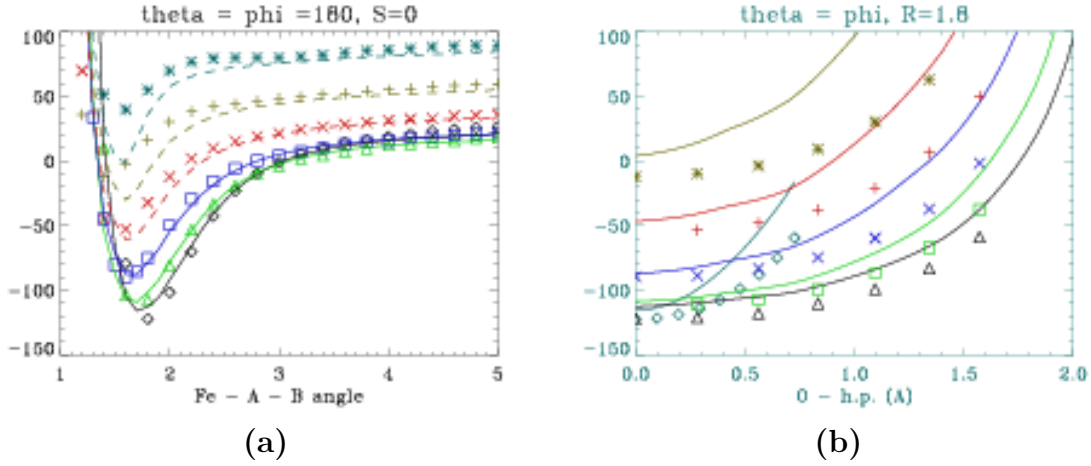
Figure 7: Energy of structures which characterize the low spin potential near the spin crossing. **(a)** $V(R)$ at different iron-heme plane distances, shown with the same symbols as in Figure 4. **(b)** $V(\phi)$ for $\theta = 180$ (diamonds), and for $\theta = \phi$ at different iron-heme plane distances, $d=0.0$ Å, (triangles); 0.1 Å, (squares); 0.2 Å, (x); 0.3 Å, (+); 0.4 Å, (*), plotted as a function of the distance from the oxygen atom to the z-axis. $R=1.8$ Åand $\alpha=0$.

from tilting the entire CO away from the heme axis, with $\theta = \phi$ and $d_{Fe-C} = 1.8$, Å. We plotted both types of calculation on the same plot, as a function of oxygen-heme symmetry axis distance, to emphasize the different physical effects. Compare to the calculations of Spiro et al. [82], which explicitly included the distal histidine, but did not attempt a physical deconvolution of the calculated potential.

The d dependence of the angular (non) dependence also indicates that it is not the bonding interaction causing the increase in energy with bond tilt.

We characterized the potential only where it was important to determine where the spin crossing is for bonding, and this is also why we chose the two coordinates we did to characterize the low spin state. It is fit with the same functional form as the high spin data, as described in the next section.

Moreover, we obtain the experimentally observed (by X-ray [90]) optimum binding distance between Fe and C, 1.8 Å, and binding strength of approximately 100 kJ/mol.

4.3   Spin Crossing

Because of its central importance in the binding event, we show the spin crossing position and energy in Figure 8. The spin crossing occurs at a minimum energy when the iron is 0.1 Å out of the heme plane; this energy increases quickly as the iron moves farther out of the heme plane. On the other hand, from the parabolic potential dependence on d for $S = 2$ state it is clear that in the absence of the ligand the iron is likely to stay at $d \sim 0.25$ Å. Hence we conclude that the binding of CO to Fe in Mb must incorporate a collaborative
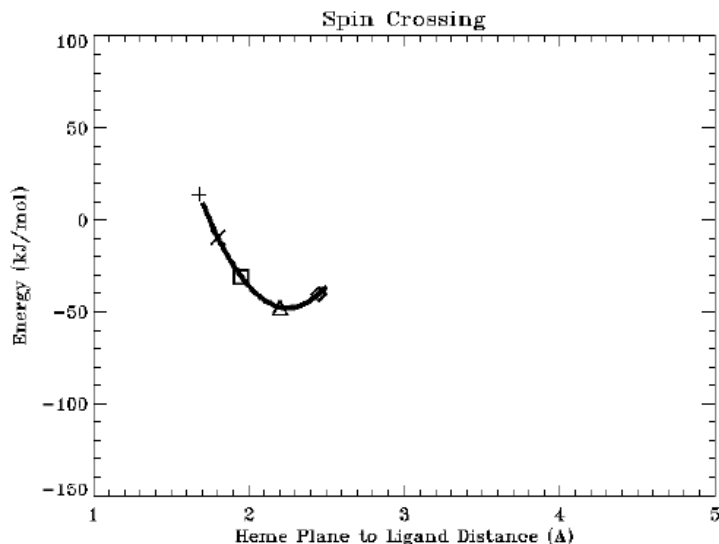
Figure 8: Energy at which the S=0 and S=2 surfaces cross plotted against R for d=0.0 Å, (diamonds); 0.1 Å, (triangles); 0.2 Å, (squares); 0.3 Å, (x); 0.4 Å, (+), for $\theta = \phi$=180 (solid line) and others. α=0 for all curves.

effort of both Fe moving into the heme-plane and CO approaching the heme plane.

4.4   Electrostatic Properties

The polarizability of the heme makes a larger energetic contribution to the energetics of typical charges moving near the heme group than does the dipole moment of the heme. The anisotropic polarizability also demonstrates that the heme behaves to some extent as a conducting plane.

The electrostatic potential derived directly from the electron density is shown in Figure 9a for the low-spin, bound configuration, and in Figure 9b for the unbound case. The cross-section is of the x-z plane. The electric field allows calculation of both the effect of ligation state on the electric field and the effect of external fields on the heme reactivity. The contour lines are separated by 2.0 V and the solid (dashed) lines correspond to positive (negative) charge. For comparison, trans-membrane gradients in biological systems are typically 100 mev over 25 Å.

Difference plots are also shown, with a smaller contour interval. It is clear that the CO is polarized when bound to the heme, in agreement with its large IR oscillator strength, compared to free gas CO, and that a large dipole moment change occurs when the iron moves relative to the heme plane.

We try to capture the essence by fitting to point charges using the CHelpG routine [14] in Gaussian 94. We use vdW radii of 0.5 Å for low spin iron, and 0.9 Å for high spin iron, which influences the results. The fit to point charges was constrained to always result in the
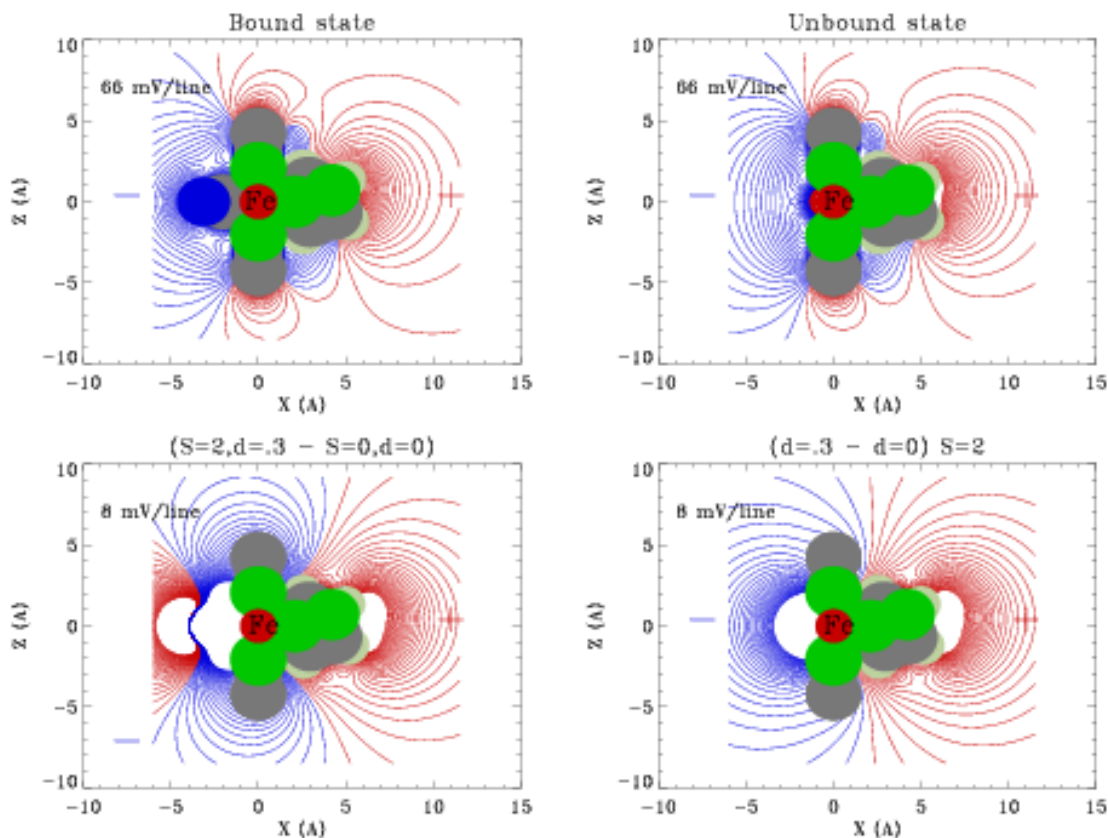
15

Figure 9: Electrostatic potential from -30 V to 30 V at 2 volts / line of the model heme-imidazole-CO group in **Upper left (a)** the low spin state, and **Upper right (b)** the high spin state, calculated from the electron density. Negative potentials are shown as dashed lines, while positive potentials are solid lines. **Lower left (c)** Change in potential due to CO binding, including the appearance of CO, the spin change, and motion of iron into the heme plane, at 0.25 volts / line. **Lower right (d)** Change in potential in the high spin state as d changes from 0.3 Åto 0.0 Å, at 0.25 volts / line.

moment	S=0 d=0	S=2 d=0
Z	0.287	0.270
XX	-0.68	-0.69
ZZ	-0.72	-0.69
XXZ	0.0782	0.035
ZZZ	-0.0349	0.054
XXXX	-1.658	-0.248
ZZZZ	-0.59	0.066
XXZZ	-0.45	0.064

Table 2: Selected multipole moments in different configurations of Heme-CO system. (Units are $e(5\text{Å})^n$, and coordinate system is rotated by 45 degrees and flipped about the z-azis. Note that the moments depend on the origin, which we take as the center of the heme plane.

dipole moment determined directly from the electron density. In order to check the validity of the fit to point charges (Table 1) in reproducing large scale charge movements in the heme group, we of course look at Figure 9, but also at the multipole moments, in Table 2, which are also calculated directly from the charge density. They are particularly useful for the heme, because it is has C_4 symmetry, so the motions appear concentrated in only a few moments.

Several interesting points can be made. The dipole moment does not change upon photodissociation, although the oxygen atom has a substantial charge when CO is bound. The dipole moment changes more with iron motion than with the spin change and CO photolysis. The quadrupole also does not change much, indicating that charge is not simply flowing between the iron and the heme plane. Quite a lot of electron density sitting in front of the heme.

The obtained potential indicates the necessity for the inclusion of all heme plane atoms into our calculation of the binding energy, as the potential in the vicinity of Fe atom is clearly strongly influenced by all of heme atoms. Second, as seen in Figure 9a, for $S = 2$ there is a non-trivial electrostatic potential in the area in between N and Fe atoms. Heme is unusual in its size and polarizability, as seen, for example, in NMR shifts of nearby atoms [61]. Electrostatic effects are also quite important to allosteric changes in hemoglobin and cytochrome c oxidase, which pumps protons across a lipid membrane.

For example, 0.2 e placed at the position of N_ϵ of H64 will be solvated much less by dipole interaction with the heme group than by the polarizability of the heme group (its image charge).

5 Fit of Interaction Potential to Model Function

The obtained results are not sufficient for anything unless we can fit them in terms of simple functions. The fit also adds considerable insight into the relative importance of component interactions. Our L-J interaction required three body interactions, while our bonding interaction required four body interactions. The fits, shown in Figure 4–6, are within $300 \text{ K} \times k_B$ for most orientations and reproduce all qualitative features of the calculation for the twelve different interactions shown. More complex fits are possible, but we like this one in part because of its relative accuracy, but especially because of its simple physical interpretation.

It is convenient to define several quantities. We denote the coordinate vector of the iron and ligand atoms by $\mathbf{r}_{Fe}$, $\mathbf{r}_C$ and $\mathbf{r}_O$, respectively. We specify the origin of our coordinate system by assuming that $\mathbf{r}_{Fe} \equiv (0, 0, -d)$, with $d > 0$, i.e., the origin is in the heme plane, right above the Fe atom.

In the equations below all lengths are in Å and all energies in kJ/mol. The fitting function contains four terms:

$$E = E_{Fe-hp} + E_q + E_{L-J} + E_{bond} \tag{3}$$

where the terms correspond to the position of iron with respect to the heme plane, the electrostatic energy, Lennard-Jones like interactions and a bonding interaction, respectively. Values of parameters are in Tables 3 and 4.

We fit the overall iron-heme plane interaction $V(d)$ to a parabola.

$$E_{Fe-hp} = b \, (d - d_{eq})^2. \tag{4}$$

5.1 Electrostatic Potential

We calculate the electrostatic interaction directly from the obtained charge densities via an appropriate interpolation, representing the experimental values of the dipole and quadrupole

	C	O	Fe_2	Fe_0	N	C$'$
R	1.8	1.75	0.9	0.5	1.85	2.0
ϵ	0.35	0.40	0.30	0.30	0.50	0.35
	0.60	0.50	2.0	—	—	—

Table 3: Lennard-Jones parameters of the phenomenological heme–CO potential used in fitting the obtained (QM) results. Units are Å and kJ/mol. The third row includes coupling of L-J parameters to other coordinates, as described in text. $R_{Fe}=.5$ in the low spin state.

	High	Spin	Low Spin
	C	O	C
V	20.0	5.0	160
c_V	60	20	150
l	1.0	1.5	0.6
c_l	1.0	0.0	1.0
σ	1.2	2.0	0.7
c_σ	-0.5	-0.5	0.0
σ_4	4.0	—	1.0
d_{eq}	.26		.1
b	300		420

Table 4: Bonding parameters of the phenomenological heme–CO potential used in fitting the obtained (QM) results. l_{Fe} is 1.2 Å. Also need angular dependence of interactions.

moment of the CO with three point charges. We cannot reproduce the electric potential near the heme with point charges on the atoms, and we cannot separate the electric field of the heme from that of the CO in the low spin state with the CO nearby. Consequently, we simply use the high spin for d=0.1 Å for all cases.

We included a term in the potential which is a three point charge CO interacting with the calculated electric potential shown in Figure 9.

$$E_q = \Sigma_{i,j} \frac{q_i q_j}{r_{ij}} \tag{5}$$

where i sums over the charge density of the heme, and j sums over the three-charge model of CO, where the point charges are -0.8 e at the C, 1.63 e at the center of the CO and -0.83 e on the oxygen [86]. These numbers reproduce the gas phase dipole and quadrupole moment of the CO. This effect produces the overlapping of the tails in the $\phi = 120$ and 150 calculations in Figure 5b and c, as well as significant attraction of CO to the iron.

We do not pretend to have separated all of the electrostatic effects. Both CO and the heme group are quite polarizable, and the heme produces relatively large electrostatic fields. These effects are included in the Lennard-Jones and bonding interactions.

5.2   Lennard-Jones

See Table 3. We denote, as usual, R_{Fe}, R_C, R_O and ε_{Fe}, ε_C and ε_O, as the hard-core repulsions and hard-core energies of Fe, C and O atoms, respectively.

For the functions plotted in Figure 4–6, the behavior at low distances is dominated by a hard-core repulsion. For all cases we have verified that the repulsion is proportional to $1/r^{12}$. The Lennard-Jones interactions used are shown in Figure 10c, with the parameters used in Table 3. The attraction is less than 1 kJ/mol for all L-J interactions. Modification to the standard MD parameters were needed.
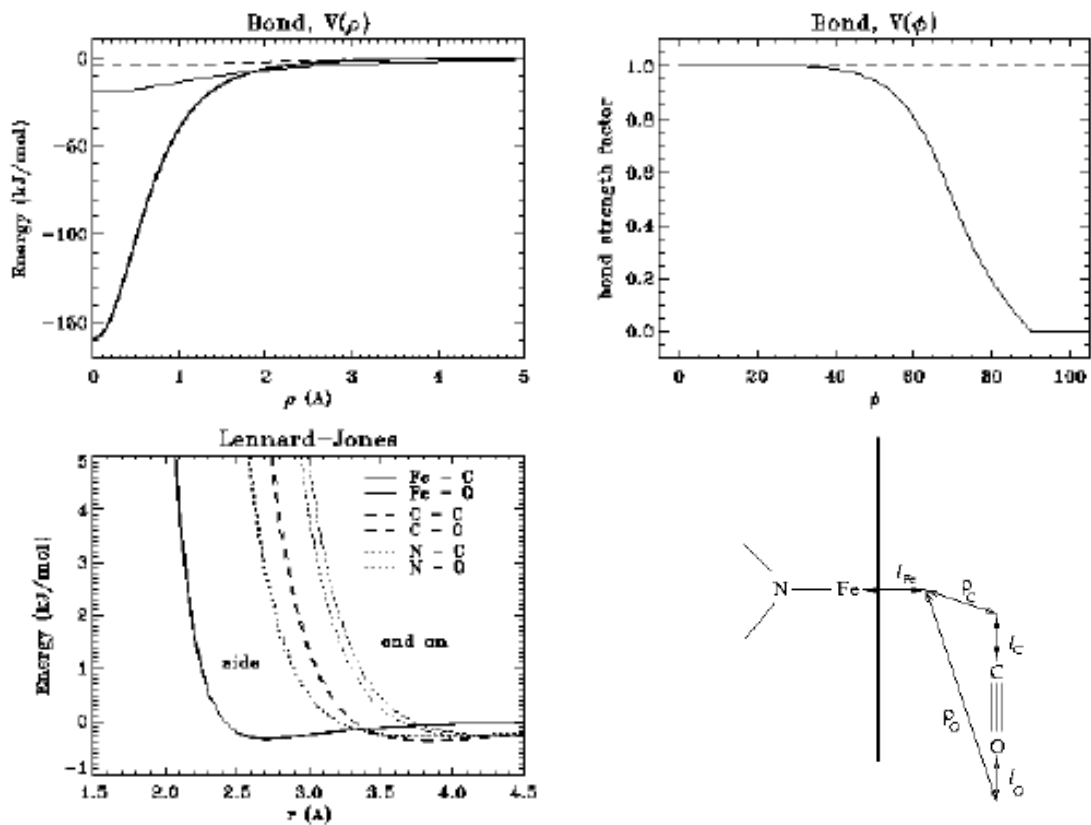
Figure 10: Component interactions which make up the model heme-CO interaction potential. **Upper left (a)** Diagram showing l and ρ, used in describing the bonding interaction. **Lower left (b)** Lennard-Jones potentials used in model function. The anisotropic interactions are shown at extreme values, and the iron-carbon interaction is shown in both spin states. **Upper right (c)** ρ dependence of bonding interaction, shown for $d=0$ in both spin states. **Lower right (d)** angular dependence of bonding interaction shown for both spin states. The functions used are described in text, and values of all parameters are in Tables 2 and 3.

The basic form of our Lennard Jones interaction follows that in established MD literature. Specifically, each atom is assigned a radius R_i and an interaction energy ϵ_i. The interaction potential is then a function of the distance between the atoms:

$$E_{L-J}(r) = \epsilon \left[\left(\frac{R}{r} \right)^{12} - 2 \left(\frac{R}{r} \right)^6 \right], \tag{6}$$

where $R = R_i + R_j$ and $\epsilon = \sqrt{\epsilon_i \epsilon_j}$, as used in both AMBER [20] and CHARMM [58]. We use this simple form for the Lennard-Jones interaction between iron and each atom of the CO. For the CO-heme carbon interaction, we used:

$$E_{L-J}(r) = 0.6\varepsilon \left[\left(\frac{0.6R}{r} \right)^{12} + \left(\frac{1.23R}{r} \right)^8 - 2 \left(\frac{1.23R}{r} \right)^6 \right], \tag{7}$$

and for nitrogen-CO,

$$E_{L-J}(r) = 0.78\varepsilon \left[\left(\frac{0.87R}{r} \right)^{12} + \left(\frac{0.9R}{r} \right)^8 - 2 \left(\frac{0.9R}{r} \right)^2 \right]. \tag{8}$$

The equations are written so that the R and ϵ correspond to a 6-12 potential of a similar shape. All potentials are plotted in Figure 10b.

We also found it necessary to include many-body effects by allowing the R_i to depend on angles. Both the carbon and the oxygen appear 0.6 Å larger when approached from the end, compared to the side. This is indicated in Figure 10c in the C-N and O-N interaction. We also made the R_{Fe} a linear function of d, and R_N depend on the Fe-N-C or O angle. All of the requisite parameters are presented in the third row of Table 3.

The shape and the spatial spreading of the optimum distances in the curves in Figure 6 indicate that the repulsion and the attraction by the heme carbons is soft and short range, respectively, which is why we chose the LJ terms specified in (7). At the same time the behavior of nitrogens is quite different: the energy dispersion at large distances of the Fe-O-C curves in Figure 4 indicates that the attractive part of the heme nitrogen-CO LJ interaction is longer ranged ($\sim 1/r^2$), as in (8).

5.3   Bonding Interaction

The Lennard-Jones interaction described does not have an attractive part. It must be provided by a specific bonding term, described here. See Table 4 for the parameters and Figure 10 for a plot of the relevant functions.

The bonding potentials are given by:

$$V_{bond} = n(\phi)B(\rho) \tag{9}$$

where:

$$n(\phi) = \frac{\frac{\pi}{2} - \phi + \eta \left(\phi - \frac{\pi}{2} \right)^4}{1 + \eta \left(\phi - \frac{\pi}{2} \right)^4} \tag{10}$$

21

and

$$B(\rho) = V \left[\frac{\left(\frac{\rho}{\sigma}\right)^2 + \left(\frac{\rho}{\sigma_4}\right)^4}{1 + \left(\frac{\rho}{\sigma}\right)^2 + \left(\frac{\rho}{\sigma_4}\right)^4} - 1 \right], \tag{11}$$

where ϕ is defined in Figure 2, ρ is defined in Figure 10d, and parameters are given in Table 4 for both the iron-carbon and iron-oxygen interaction.

It is useful that (9) factorizes. This is because of our choice of ρ, the distance between the appropriate orbitals and V is its overall magnitude (see Figure 10a) rather than simply atom centered potentials. Note that this form of the interaction has correct limiting behavior for both $\rho \to 0$ (where $B \sim \rho^2$) and $\rho \to \infty$ (where $B \to 0$). The short range (quadratic) and the long range dependences are determined via the lengths σ and σ_4 respectively.

The dependence of both the energies and the lengths σ_C and σ_O on d has been assumed to be quadratic, with slopes c_i, $i = 1, 4$ given in Table 4. The angular dependence of the Fe–C bonding is shown in Figure 10b, while the Fe–O bonding is assumed to be isotropic.

The last arguments of the bonding interactions are given by the distances between Fe and CO binding orbitals (denoted as ρ_C and ρ_O respectively), where the C and O orbital directions are assumed to be specified by $\vec{\ell}_{CO}$, as shown in Figure 10. In the case of Fe-C bonding one further complication arises: the minimum of the Fe-C bond potential is not spherically symmetric, as is evident by comparing the binding by rotation plot (Figure 6) with the radial dependence of the bonding function (Figure 4 and b). Hence we have set

$$\rho_C^2 = (\rho_{Cx}^2 + \rho_{Cy}^2) \left(1 + \frac{c_5 \sqrt{x_C^2 + y_C^2}}{1 + (x_C^2 + y_C^2)^5} \right)^2 + \rho_{Cz}^2 \tag{12}$$

where c_5 is the fitting parameter (see Table 4).

The attraction of the iron for the CO is summarized in Figure 10. It is clear from the first two panels that the bonding to the carbon is much stronger than the bonding to oxygen. The angular dependence is shown in Figure 4b. The iron-carbon bonding interaction varies very little for $\phi \sim \pi$, when $\theta \sim \pi$, and very rapidly for $\phi \sim \pi/2$, where it approximately vanishes. Hence our use of (10). The iron-oxygen bonding interaction is isotropic. This difference can be seen in the DFT calculations by comparing Figure 4c and d.

Discarding the atom center potential in favor of the 'orbital' centered bonding potential shown in Figure 10d greatly increases the simplicity of combining angular and radial dependence. Although the bonding interaction is clearly symmetric, it is added to a Lennard Jones interaction, described above, so that the asymetric functions shown in Figure 4a and b are accurately reproduced. The center of the potential is harmonic, with a different frequency along the heme axis compared to within the heme plane, given by (12). The unusual decay with $\frac{1}{r^2}$ may originate from van der Waals attraction of a fluctuating dipole (CO) to a large plane (the heme).

All of this is consistent with a picture where the bond is formed by overlap of iron orbitals with ligand orbitals. The bond is much stronger in the low spin case because the strongly overlapping orbitals can be doubly occupied, albeit at the cost of spin pairing energy. In the

case of carbon, the orbitals are directed along the CO axis. In the case of oxygen, there are several possible orientations which interact equally, as expected by, for example, the tilted orientation of O_2 when it is bonded to model heme compounds.

The bonding interaction depends on the iron-heme plane distance in several ways, as seen in Figure 10a and b. It is considerably stronger when $d \sim 0$, reaching almost 30 kJ/mol. When the iron is .5 Å out of the heme plane, the bond strength is just under 10 kJ/mol. The bond length and width are also allowed to vary linearly with d.

5.4 Fit to Low Spin Potential

Fits to the low spin potential are shown in Figure 7, and parameters describing the fit are given in Table 4, using the same functional form already described for the high spin potential. We see that the bond becomes much stronger and narrower, the equilibrium iron out of plane distance decreases, the Lennard-Jones radius decreases, and the dependence of paramenters on d changes, but all else is the same. Figure 10a shows most of the changes.

This similarity in functional form of the high and low spin state provides credibility to the physical decomposition of the calculated potential into component interactions. It also suggts that it may be possible to treat systems with many important spin states semi-empirically.

6 CO Motion in Frozen Sperm Whale Myoglobin

Figure 11 shows the heme pocket of myoglobin from the 20 K photoproduct of CO photolysis, determined by x-ray crystallography [78], with protons added by a utility program of AMBER. Motion of the CO to the heme iron is directly governed by the five amino acids shown, while H93 controls iron motion away from the heme plane. We first consider CO motion in this pocket with protein atoms fixed in their averaged positions determined by the x-ray data, using both the fit potential we have developed and established MD parameters.

The 'reaction plane' is visible in Figure 11. With the exception of H64, the conserved amino acids are hydrophobic, and so have only Lennard Jones interactions with the CO; electrostatics plays a significant role in determining the CO energy only when it approaches the iron atom. The B-site is well defined, and in agreement with the x-ray data, while steric hindrance to recombination is provided by N_ϵ of H64 and C_δ of V68.

We begin our quantitative treatment of CO motion in the heme pocket in Figure 12 by confining the CO to a plane, optimizing for orientation, and plotting its potential energy vs. center of mass position of the CO. This plane is a zoomed in version of Figure 11, and quantifies the potential energy surface on which the CO moves. Note that this figure can be made directly from a PDB file. The B-site is a clear minimum in energy, and it is seen to require 35 kJ/mol to move the CO to the spin crossing.
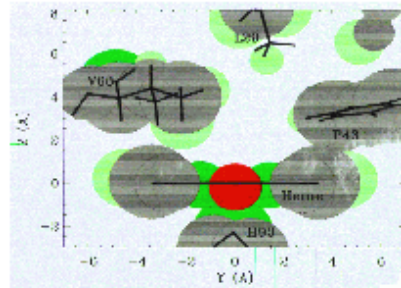
Our three biggest assumptions are the use of the planar heme potential, confining the CO to a plane as it moves about the protein, and ignoring electrostatic interactions of the CO
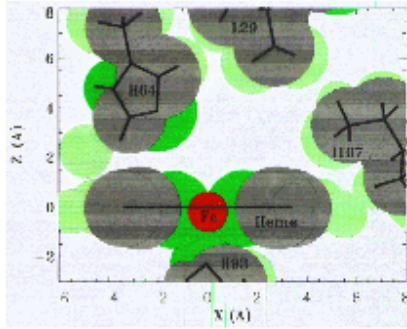
(a)
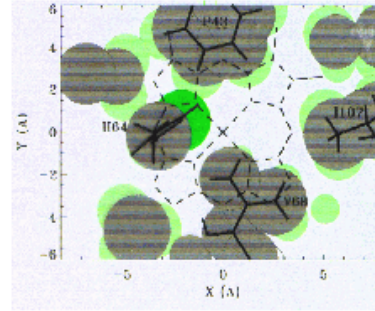
(b)

(c)

Figure 11: Cross sections through the active site of sperm whale myoglobin after photodissociation of CO at 20 K [78], with protons added by AMBER. The planes are given by **(a)** y=0.3 Å, **(b)** z=3.0 Å, and **(c)** x=?. Atoms are shown to the radius at which the LJ interaction = 0.
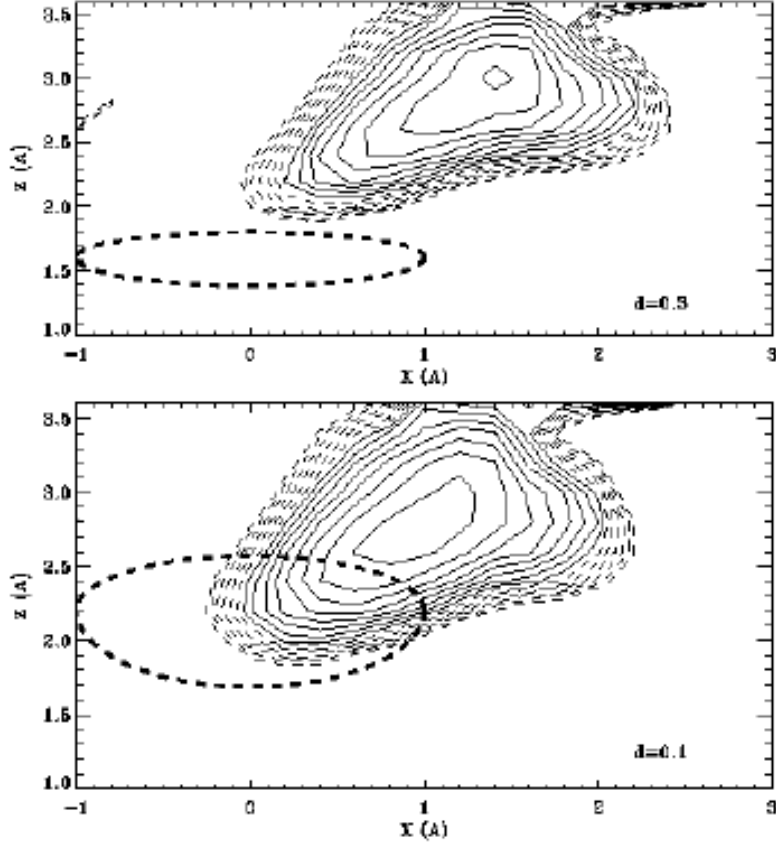
Figure 12: Contour plot of potential for CO moving around heme pocket of CO photoproduct myoglobin in **top (a):** equilibrium structure and **bottom (b):** a proposed transition state structure obtained by shifting the protein atoms 0.2 Å in the x direction and 0.1 Å in the y direction. Protein coordinates are taken from the sw MbCO xray structure of Schlicting et al.

with the amino acids of the distal pocket. We feel that none of the assumptions eliminate essential physics involved in binding, and only weakly affect the quantitative result. They are certainly essential in making this calculation feasible, and so we postpone their justification to the discussion section, along with other nasties which we encounter along the way.

If only CO is allowed to move, binding will be governed by the potential shown in Figure 12a, assuming the pocket is 1.5 Å across and the CO has thermal energy, the CO will travel back and forth across the pocket 10^{12} times per second at 100 K ($\frac{1}{2}mv^2 = 100k_B$; $A_0 = v/3$ Å. We then expect the following:

$$k(T) = \frac{A_0}{f_e f_o}\sqrt{\frac{T}{100 \ K}} \exp\left(-\frac{H_0}{k_B T}\right) \tag{13}$$

where $A_0 = 1 \times 10^{12}$ s^{-1}, $H_0 = 35$ kJ/mol, f_e is a factor describing how often the CO is rejected by a slow electronic state change, and f_o is a factor describing how often the CO

25

is in the correct orientation upon collision with H64. Care is required to define a binding 'attempt'.

This approach provides a starting point to our treatment of the binding process; binding occurs with motion of the protein and heme atoms, and not just the CO. It defines H_0, the activation enthalpy for the CO to bind to 'frozen' protein, and gives a physical meaning to A_0, the frequency at which the CO crosses the heme pocket. Treatment of vibrational motion builds upon this model, it does not replace it.

Figure 12 shows the potential of the heme pocket in a proposed transition state. H_0 has changed because of motions of at least three independent coordinates — d, x, and y. We quantify this dependence before presenting our model of low temperature binding.

6.1 Dependence on Heme Configuration — d

In Figure 12, we see that the largest effect of decreasing d to 0.1 Å is to move the spin crossing further from the iron atom, where it is much more accessible to the CO. There is not much change in the high spin potential. We can repeat this procedure and plot H_0 as a function of d, the iron out of plane distance. This is shown as the dotted line in Figure 13.

Most of the change in energy is of the low spin state decreasing in energy — an effect unique to this coordinate.

6.2 Dependence on Protein Configuration — x, y

N_ϵ of H64 and C_δ of V68 sterically hinder access of CO to the heme iron atom. We estimate the effect of the position of these atoms on H_0 by simply sliding the entire distal pocket relative to the heme group (in reality, motion of these groups needs to be projected onto this coordinate, but this is not difficult). We plot both effects in Figure 12d that the shape of the potential changes significantly, and, again, we plot the above-defined H_0 vs. displacement in the x and y directions in Figure 13 as dashed and solid lines, respectively.

For y, we must redefine our reaction plane, and we see that little is gained by centering the heme in the pocket better, but much is lost by continued motion of the heme under V68. As expected from the binding by rotation plots in Figure 6, the barrier changes by many $k_B T$ with displacements of only ~ 0.1 Å, at least in a protein with completely motionless atoms.

7 Microscopic Model of Binding

We now present a microscopic model of binding, based on the following assumptions.

(1) Nuclear motion is classical.

(2) CO binds to the iron at the crossing of the low and high spin potential surfaces, and non-adiabaticity of electron motion is taken into account with a multiplicative factor — the success rate of spin crossing.

(3) Motion is entirely vibrational at low temperature, and a combination of vibrational motion and conformational changes at physiological temperature.

(4) The various vibrational and conformational motions which influence the recombination barrier are independent of one another. This occurs if the collision time of CO with the iron atom is faster than any of the vibrations which modulate the barrier.

To quantify the effect of vibrational motion of iron and the protein we consider a simple model of a vibrational coordinate which modulates the enthalpy barrier to recombination according to the equation:

$$H = H_0 + H_{mod} \cos \omega t \tag{14}$$

The rate, averaged over an entire vibrational cycle is then:

$$< k(t) > = A_0 \exp(-\frac{H_0}{k_B T}) \frac{1}{2\pi} \int_0^{2\pi} \exp\left(-\frac{H_{mod}}{k_b T} \cos \omega t\right) d\omega t \tag{15}$$

which is [1]:

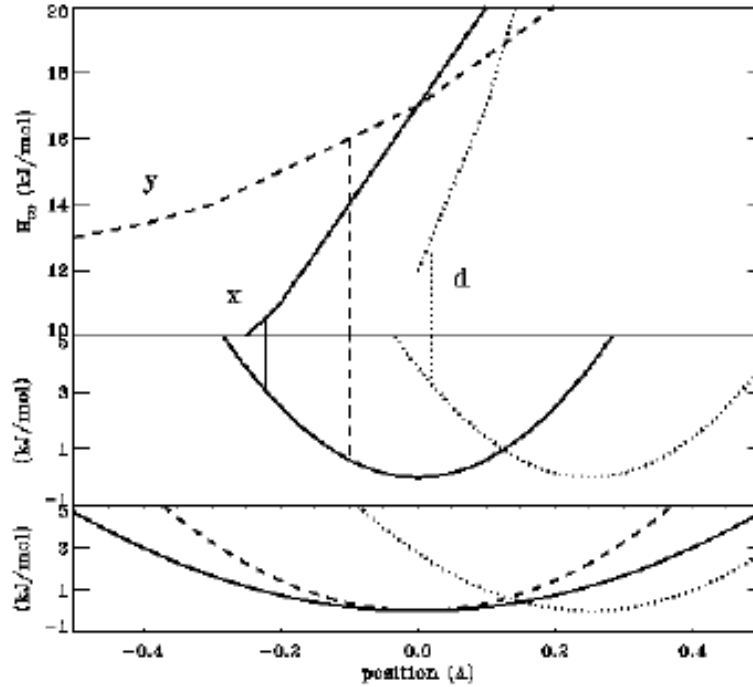$$A_0 \exp\left(-\frac{H_0}{k_B T}\right) I_0 \left(\frac{H_{mod}}{k_B T}\right), \tag{16}$$

Figure 13: **Top (a)** Effect of motion of the heme in the x and y direction and iron motion relative to the heme plane on the activation enthalpy of rebinding. Activation enthalpy is defined simply as the difference between the energy at the minimum of the 'B' site and the spin crossing. **Middle (b)** Potential describing vibrational motions along d, x, and y. **Bottom (c)** Potential describing conformational motions along d, x, and y.
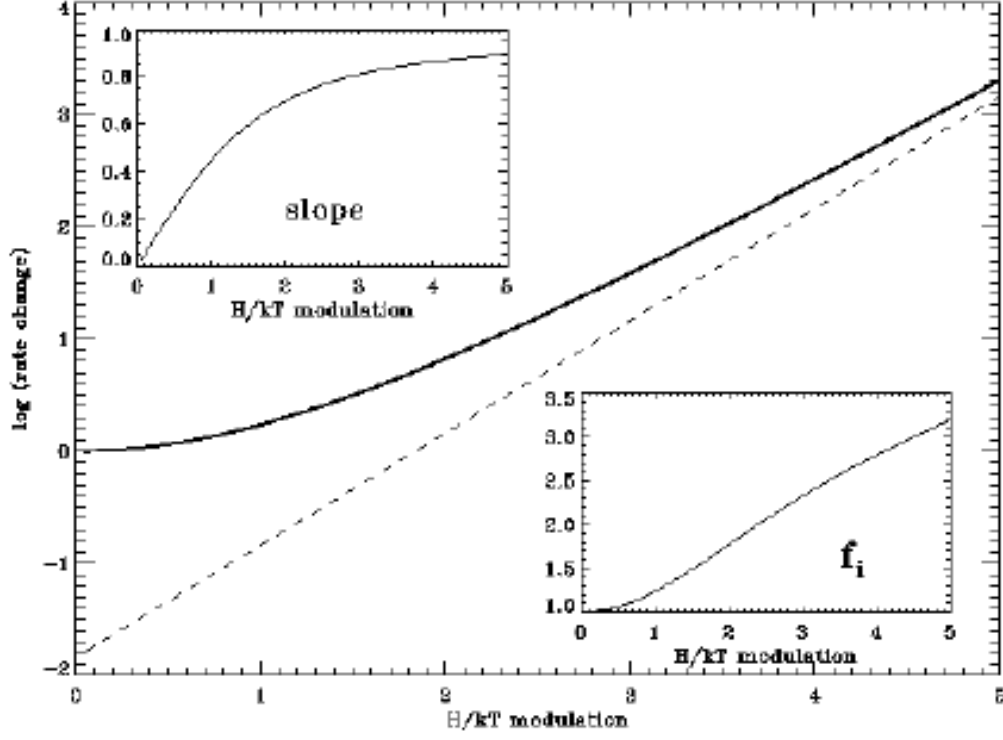
27

Figure 14: Effect of vibrational modulation of enthalpy barrier on observed activation enthalpy, as described in text.

where I_0 is the modified Bessel function, which is plotted in Figure 14.

Vibrational (T < 160 K) dynamics will cause each component to contribute to both the activation enthalpy pre-exponential factor. Consider, for example, a mode which cause the barrier to change by two $k_B T$ during a vibrational cycle; the binding rate will be more than an order of magnitude faster during one half than the other. The fastest binding will occur if the CO simply waits for the proper phase (factor two slowing) instead of waiting for the random placement of thermal energy in the mode to reach the barrier at the average configuration. One simply looks at the slope of this curve to estimate the apparent activation enthalpy change and the intercept to find the reduction in the pre-exponential factor. The slope and intercept are plotted as insets in Figure 14.

For each vibrational mode which affects H, the enthalpy barrier will be reduced by an amount H_i, the pre-exponential is reduced by a factor $1/f_i$, and the overall expression for the temperature dependence of the rate becomes:

$$k(T) = \frac{A_0}{f_e f_o} \frac{T}{100 \ K} \exp\left(-\frac{H_0}{k_B T}\right) \Pi_i \frac{1}{f_i} \exp\left(\frac{H_i}{k_B T}\right) \tag{17}$$
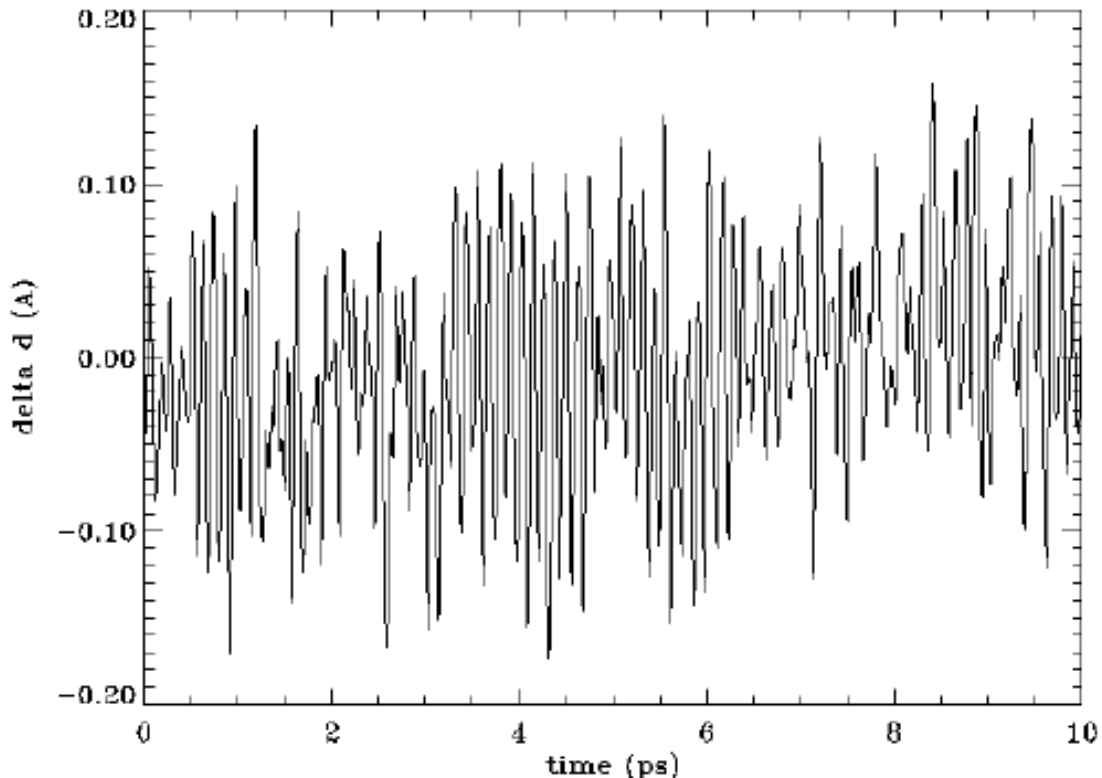
28

Figure 15: Motion of the iron atom perpendicular to the heme plane, taken from a molecular dynamics simulation.

7.1 Vibrational Motion

In order to apply (17), we need an estimate how large H_{mod} is for each coordinate, d, x, and y, as well as the number of normal modes which contribute to each. Figure 15 is sufficient to show the character all of the vibrational modes involved. It is a plot of d as a function of time for 5 ps of an MD simulation of fully solvated myoglobin. It is clear that this motion involves several normal modes; similar plots can be made for motion along x and y.

Motion along d should include several effects, such as distortion of the heme plane and vibration of iron, relative to the imidazole ring, and possibly even effects of the electric field — any vibration which influences the spin crossing postion or the iron-heme plane distance. Likewise, x and y include motions of the proton on N_ϵ of H64, vibration of the imidazole ring, and bending motions involving the α, β, and γ carbons of H64, plus vibrations of the E helix relative the the heme group. Basically, we are just calculating the motions involved in getting the protein-CO system into its transition state, which Zheng et al. [94] have already pointed out involves many modes, and projecting it on to these three coordinates.

Treating vibrations in this way is similar to the softening of the potential which occurs by letting the heme relax during the DFT calculations, but has two important advantages.

29

First, it greatly simplifies the DFT calculation by eliminating degrees of freedom which are best characterized by X-ray diffraction and Raman scattering. Second, it allows the unique vibrational character along each coordinate, due to the complexity of the protein structure, to appear clearly in the calculation. The effect of the complex vibrational motion (stretching, bending, and twisting) is characterized by the amplitude and number of normal mode for d, x, and y, as well as the sensitivity of the enthalpy barrier to each coordinate.

It is not known how large the vibrations of interest are. We take the slope of the inelastic neutron scattering mean square displacement vs. temperature between 50 and 160 K [22] to give the vibrational potential along d, x, and y. The potential derived from this data is shown in Figure 13b, with d described by the dotted line, x by the solid, and y by the dashed line. To determine how much of the activation enthalpy goes into each mode, simply match the slopes in Figure 13a and b, as indicated by the vertical lines. Thus we see that adding energies of 4.5, 3, and 1 kJ/mol results in H_{mod} values of 13, 4.5, and 2 kJ/mol for d, x, and y, respectively.

Much work has addressed the amplitude of vibrational motions, [31, 47, 80, 62, 84], but each suffers from at least one problem which makes it impossible to directly apply to this calculation.

7.2   Size of Barrier in the Presence of Vibrational Motion

Figure 14 illustrates the effect of (16) on both the activation enthalpy and the pre-exponential factor. In principle, one could solve this problem by running a molecular dynamics simulation, but then the component interactions are difficult to separate, and a new simulation needs to be run for each proposed simulation. At high temperatures, all the non-harmonic modes of the protein will be activated and the CO will simply escape, while at low temperature, the MD simulation will not be representative of the variety of conformations in which the protein may be found.

We assume three normal modes contribute to d, 2 to x, and 1 to y. Using Figure 14, we find f_i is 3^3, 1.9^2 and 1.8, for d, x, and y, respectively, while the value of H_{CO} needed for x = y = 0 of 11 kJ/mol is reduced by 6 and 2 kJ/mol by x and y, meaning only 3 kJ/mol is needed to move the CO to the spin crossing.

The total activation enthalpy for recombination, 11.5 kJ/mol, is composed of four contributions: 4.5 kJ/mol to move the iron relative to the heme plane, 3 kJ/mol to move the heme relative to N_ϵ of H64, 1 kJ/mol to move the heme relative to C_γ of V68, and 3 kJ/mol to move the CO to the spin crossing, as indicated in Table 5. If the pre-exponential reduction factor plot in Figure 14 were linear, it would not matter how many modes the vibrational modes were factored into, but since it is, it does.

The pre-exponential factor, 10^9 s^{-1} is reproduced by the time for the CO to bounce back and forth across the heme pocket, 1×10^{12} s^{-1} reduced by factors of 27, 3.6, and 1.8 by d, x, and y and an orientation factor of 5 (perhaps including some non-adiabaticity), which explains how often the CO is oriented properly for binding. You could call the whole thing entropy if you like, but then you lose physical understanding of the components.

coord	displacement	modes	H	ΔH_{mod}	f_i	δH	f_i
x	.25	2	3	4.5	1.9, 1.9	3	2, 2
y	.10	1	1	2	1.8	1	1.8
d	.15	3	4.5	13	3, 3, 3	6	3.15, 3.15, 3.15
CO	—	—	4		5		5
total	—	6	11.5		900	21.5	1125

Table 5: Possible contributions of structural coordinates to the rebinding barrier. All energies are in kJ/mol and all distances are in Å. Changing conformation of x is also likely to affect f_0. δH is the change in H resulting from a 0.1 Å increase in each coordinate's equilibrium, and the f_i are the new values for the reduction factors.

7.3   Low Temperature Distributions

The extent of conformational distribution can be determined by looking at the anisotropic B factors [90] or the temperature dependence of mean squared displacements [22]. This distribution is anharmonic and much more dependent on the overall construction of the protein than vibrational motion. Following experiment, we construct the potential curves shown in Figure 13 c. The extent of these distributions is approximately 0.5 Å, RMS, and is dependent on entirely different phenomenon than the potential of vibration. The heme position, for example, is distributed in position more within its plane than along the z-axis.

Low temperature distributions are given by a thermal distribution in each potential, and the activation enthalpy for CO recombination can be estimated by matching the slope in Figures 13 a and c, similar to what was done with the vibrational motion.

These distributions provide a check on the accuracy of our calculation and model, because the width of this distribution in both real space [90] and activation energy space (Figure 1) are known.

Other distributions, such as the effect of protonating H64 or H97 are also well characterized [42, 65], and such experiments form part of the basis for the specific shape of the potentials sketched in Figure 13 c.

7.4   Relaxation

CO recombination to myoglobin at room temmperature does not occur to a protein in the 'photoproduct' structure used in the above calculations. The protein relaxes to the 'deoxy' conformation, which has a potential for ligand motion shown in Figure 16 a.

Comparison of the x-ray structure of myoglobin in the photoproduct state and the deoxy-state reveals the following changes [90]. First, the CO is missing from the distal pocket. Second, this pocket is occupied by water. Third, the heme has slid under H64 and V68, as expected from the release of strain upon photodissociation, apparently increasing H by 20 kJ/mol.
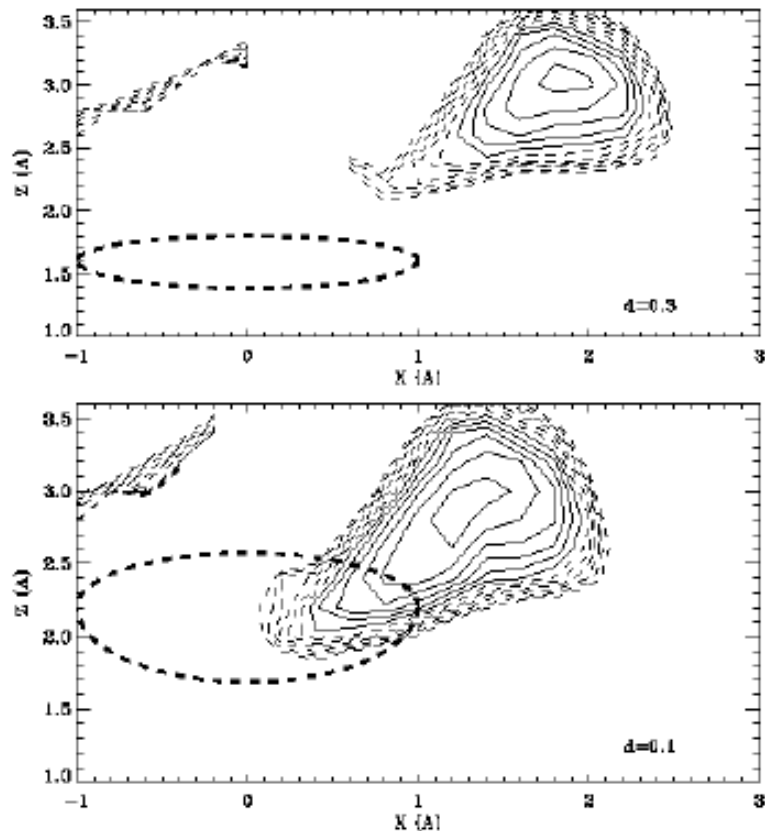
Figure 16: Contour plot of potential for CO moving around heme pocket of deoxy myoglobin in **top (a):** equilibrium structure and **bottom (b):** a proposed transition state structure obtained by shifting the protein atoms 0.4 Å in the x direction and 0.2 Å in the y direction. Protein coordinates are taken from the sw deoxyMb xray structure of Vojtechovský et al.

This apparent increase in H disappears, however, when conformational motions are allowed, as determined with the help of Figure 13. A transition state for room temperature recombination of CO is proposed in Figure 16 b.

Although this figure clearly shows a local maximum in the energy as the CO makes its way to the iron atom, it is not *a priori* clear that this is the transition state to the recombination reaction. Other events, such as slow conformational changes of particular amino acids, exiting of a water molecule from the heme pocket, or migration of CO within the protein each can potentially be a rate limiting step to room temperature recombination.

8   Conclusions

We have presented a method of solution to a long-standing problem in molecular biology: given the structure of a protein, is it possible to calculate its function? The biggest difficulty

in this solution is characterizing the conformational motions of the protein. When studying CO binding to myoglobin, it is possible to connect our calculation to experiment at many steps along the way from low temperatures, where motions are vibrational and recombination involves only small motions — to room temperature recombination, where CO and solvent motions occur, as well as changes in the tertiary structure of myoglobin.

Our simple-minded model of recombination quantitatively reproduces the low temperature barrier to CO recombination, yet is flexible enough to be extrapolated to room temperature, guided by a variety of experimental data. The iron-ligand potential has been parametrized in terms of relatively simple 3-body Lennard-Jones-like interactions and a 4-body bonding interaction. This general approach should work with other protein ligand systems.

The unually low pre-exponential factor to CO recombination can be rationalized by the synchronous motion of 5 different vibrational modes, in order for the transition state to have a reasonably low value.

The electrostatic field of the heme group cannot be modeled by atom centered point charges, and polarization of the heme is of more importance in calculating interaction energies of point charges than the unperturbed dipole field. Changes in this field are non-trivial when the iron moves relative to the heme plane.

References

[1] Abramowitz, M. and I.A. Stegun **Handbook of Mathematical Functions** Dover, New York, 1955.

[2] Agmon, N. and J.J. Hopfield, "Transient kinetics of chemical reactions with bounded diffusion perpendicular to the reaction coordinate: Intramolecular processes with slow conformational changes," *J. Chem. Phys.* 78:6947–6959, 1983.

[3] Alben, J.O., et al. "Isotope effect in molecular tunneling" *Phys. Rev. Lett.* 44:1157–1160 (1980).

[4] Alben, J.O., et al. "Infrared spectroscopy of photodissociated carboxymyoglobin at low temperatures" *Proc. Natl. Acad. Sci. USA* 79:3744–3748, 1982.

[5] Allured, V.S., C.M. Kelly, and C.R. Landis "SHAPES empirical force field: new treatment of angular potentials and its application to square-planar transition-metal complexes" *J. Am. Chem. Soc.* 113:1–12, 1991.

[6] Austin, R.H., et al. "Dynamics of ligand binding to myoglobin" *Biochem.* 14:5355, 1975.

[7] Baerends, E.J. and O.V. Gritsenko, "A quantum chemical view of density functional theory." *J. Phys. Chem. A* 101:5383–5403, 1997.

[8] Barkigia, K.M., D.J. Nurco, M.W. Renner, D. Melamed, K.M. Smith, and J. Fajer "Multiconformational surfaces in porphyrins: previews into excited-state landscapes" *J. Phys. Chem. B* 102:322–326, 1998.

[9] Bayly, C.I., P. Cieplak, W.D. Cornell, and P.A. Kollman "A well-behaved electrostatic potential based method using charge restraints for deriving atomic charges: The RESP model." J. Phys. Chem. 97:10269–10280, 1993.

[10] Beece, D. et al. "Solvent viscosity and protein dynamics" *Biochem.* 19:5147–5157, 1980.

[11] Becke, A.D., "Density-functional thermochemistry. III. The role of exact exchange" *J. Chem. Phys.* 98:5648–5652, 1993.

[12] Bhattacharya, S., S.F. Sukits, K.L. MacLaughlin, and J.T.J. Lecomte, "The tautomeric state of histidines in myoglobin" *Biophys. J.* 73:3230–3240, 1997.

[13] Bray, M.R., R.J. Deeth, and V.J. Paget, "Kinetics and mechanism in transition metal chemistry: A computational perspective." *Prog. Reaction Kinetics* 21:169–214, 1996.

[14] Breneman, C.M. and K.M. Wilberg, "Determining atom-centered monopoles from molecular electrostatic potentials. The need for high sampling density in formamide conformational analysis" *J. Comp. Chem.* 11:361–373 1990.

[15] Carlson, M.L., R.M. Regan, and Q.H. Gibson "Distal cavity fluctuations in myoglobin: protein motion and ligand diffusion" *Biochem.* 35:1125–1136, 1996.

[16] Carrero, J., D.M. Jameson, E. Gratton, "Oxygen penetration and diffusion into myoglobin revealed by quenching of zincprotoporphyrin IX fluorescence" *Biophys. Chem.* 54:143–154, 1995.

[17] Case, D.A., B.H. Huynh, and M. Karplus, "Binding of oxygen and carbon monoxide to hemoglobin. An analysis of the ground and excited states" *J. Am. Chem. Soc.* 101:4433–4453, 1979.

[18] Cheng, X. and B.P. Schoenborn, "Neutron diffraction study of carbonmonoxymyoglobin" *J. Mol. Biol.* 220:381–399, 1991.

[19] Collman, J.P., J.I. Brauman, T.R. Halbert, and K.S. Suslick "Nature of O_2 and CO binding to metalloporphyrins and heme proteins" *Proc. Natl. Acad. Sci. USA* 73:3333–3337, 1976.

[20] Cornell et al., "A second generation force field for the simulation of proteins, nucleic acids, and organic molecules" *JACS* 117:5179, 1995.

[21] Deeth, R., "Chemical choreography." *New Scientist* 155(#2089):24–27, 1997.

[22] Doster, W., S. Cusack, and W. Petry "Dynamical transition of myoglobin revealed by inelastic neutron scattering" *Nature* 337:754–756 (1989).

[23] Du, P. and G.H. Loew, "Theoretical study of model compound I complexes of horseradish peroxidase and catalase" *Bioph. J.* 68:69–80, 1995.

[24] Edwards, W.D., B. Weiner, and M.C. Zerner "On the low-lying states and electronic spectroscopy of iron(II) porphine" *J. Am. Chem. Soc.* 108:2196–2204, 1986.

[25] Eaton, W.A., L.K. Hanson, P.J. Stephens, J.C. Sutherland, and J.B.R. Dunn "Optical spectra of oxy- and deoxyhemoglobin" *J. Am. Chem. Soc.* 100:4991–5003, 1978.

[26] Ferrenberg, A.M. and R.H. Swendsen "Optimized monte carlo data analysis" *Phys. Rev. Lett.* 63:1195–1198 1989.

[27] Frauenfelder, H., G.A. Petsko, and D. Tsernoglou, "Temperature-dependent X–ray diffraction as a probe of protein structural dynamics" *Nature* 280:558–563 (1979).

[28] Frauenfelder, H. and P.G. Wolynes "Rate theories and Puzzles of hemeprotein kinetics." *Science* 229:337–345, 1985.

[29] García, A.E., J.A. Krumhansl, and H. Frauenfelder "Variations on a theme by Debye and Waller: from simple crystals to proteins" *PROT. Struct., Funct., and Gen.* 29:153–160 (1997).

[30] Ghosh, A. and D.F. Bocian, "Carbonyl tilting and bending potential energy surface of carbon monoxyhemes" *J. Phys. Chem.* 100:6363–6367, 1996.

[31] Go, N. Y. Noguti, and T. Nisikawa, "Dynamics of a small globular protein in terms of low-frequency vibrational modes" *Proc. Natl. Acad. Sci. USA* 80:3696–3700, 1983.

[32] Godbout, N., R. Havlin, R. Salzmann, P.G. Debrunner, and E. Oldfield, "Iron-57 NMR chemical shifts and Mössbauer quadrupole splittings in metalloporphyrins, ferocytochrome c, and myoglobins: A density functional theory investigation." *J. Phys. Chem. A* 102:2342–2350, 1997.

[33] Gouterman, M. "Study of the effects of substitution on the absorption spectra of porphin" *J. Chem. Phys.* 30:1139–1161, 1959.

[34] Greenwood, N.N. and A. Earnshaw, "Chemistry of the elements" Pergamon Press, New York, (1984).

[35] Guarrera, L., G. Colotti, A. Boffi, E. Chiancone, T.K. Das, D.L. Rousseau, and Q.H. Gibson, "The apolar distal histidine mutant (His69 $\rightarrow$ Val) of the homodimeric *scapharca* hemoglobin is in an *R*-like conformation" *Biochem.* 37:5608–5615, 1998.

[36] Hänggi, P., P. Talkner, and M. Borkovec, "Reaction-rate theory: fifty years after Kramers" *Rev. Mod. Phys.* 62:251–341. 1990.

[37] Harris, D., G. Loew, and L. Waskell, "Structure and spectra of ferrous dioxygen and reduced ferrous dioxygen model cytochrome P450." *J. Am. Chem. Soc.* 120:4308–4318, 1998.

[38] Hartmann, H. et al., *PNAS USA* 93:7013–7016, 1996.

[39] Hendrich, M.P. and P.G. Debrunner "Integer-spin electron paramagnetic resonance of iron proteins" *Biophys. J.* 56:489–506, 1989.

[40] Jewsbury, P. and T. Kitagawa, "Distal residue—CO interaction in carbonmonoxy myoglobins: a molecular dynamics study of three distal mutants" *Biophys J.* 68:1283–1294, 1995.

[41] Jewsbury, P., S. Yamamoto, T. Minato, M. Saito, and T. Kitagawa, "The proximal residue largely determines the CO distortion in carbon monoxy globin proteins. An *ab initio* study of a heme prosthetic unit." *J. Phys. Chem.* 99:12677-12685, 1995.

[42] Johnson, J.B., D.C. Lamb, H. Frauenfelder, J.D. Müller, B. McMahon, G.U. Nienhaus, R.D. Young "Ligand binding to heme proteins. VI. Interconversion of taxonomic substates in carbonmonoxymyoglobin" *Biophys. J.* 71:1563–1573, 1996.

[43] Kirchner, R.F. and G.H. Loew "Semiempirical calculations of model oxyheme: variation of calculated electromagnetic properties with electronic configuration and oxygen geometry" *J. Am. Chem. Soc.* 99:4639–4647, 1977.

[44] Kleinert, T., W. Dostor, H. Leyser, W. Petry, V. Schwarz, and M. Settles, "Solvent composition and viscosity effects on the kinetics of CO binding to horse myoglobin" *Biochem.* 37:717–733, 1998.

[45] Kollman, P.A., Y. Duan "Pathways to a protein — folding intermediate observed in a 1-microsecond simulation in aqueous solution" *Science* 282:740–744, 1998.

[46] Kozlowski, P.M., T.G. Spiro, A.Bérces, and M.Z. Zgierski, "Low-lying spin states of iron(II) porphine." *J. Phys. Chem. B* 102:2603–2608 (1998).

[47] Kuczera, K., J. Kuriyan, and M. Karplus, "Temperature dependence of the structure and dynamics of myoglobin" *J. Mol. Biol.* 213:351–373, 1990.

[48] Kumar, S., D. Bouzida, R.H. Swendsen, P.A. Kollman, and J. Rosenberg, "The weighted histogram analysis method for free-energy calculations on biomolecules. I. The method." *J. Comp. Chem.* 13:1011–1021, 1992.

[49] Kumar, S. J.M. Rosenberg, D. Bouzida, R.H. Swendsen, P.A. Kollman, "Multidimensional free-energy calculations using the weighted histogram analysis method." *J. Comp. Chem.* 16:1339–1350 1995.

[50] Kuriyan, J., S. Wilz, M. Karplus, and G. Petsko, "X-ray structure and refinement of carbon-monoxy (FeII)-myoglobin at 1.5 Å resolution" *J. Mol. Biol.* 192:133–154, 1986.

[51] Kushkuley, B. and S.S. Stavrov "Theoretical study of the distal-side steric and electrostatic effects on the vibrational characteristics of the FeCO unit of the carbonylheme proteins and their models" *Bioph. J.* 70:1214–1229, 1996.

[52] Kushkuley, B. and S.S. Stavrov "Theoretical study of the electrostatic and steric effects on the spectroscopic characteristics of the metal-ligand unit of heme proteins. 2. C-O vibrational frequencies, ^{17}O isotopic chemical shifts and nuclear quadrupole coupling constants" *Biophys. J.* 72:899–912, 1997.

[53] Kutý, M., J. Damborský, M. Prokop, and J. Koca, "A molecular modeling study of the catalytic mechanism of haloalkane dehalogenase. 2. Quantum chemical study of complete reaction mechanism" *J. Chem. Inf. Comput. Sci.* 38:736–741, 1998.

[54] Lamb, D.C., V. Prusakov, N. Engler, A. Ostermann, P. Schellenberg, F.G. Parak, and G.U. Nienhaus "Photodissociation and rebinding of H_2O to ferrous sperm whale myoglobin" *J. Am. Chem. Soc.* 2981–2982, 1998.

[55] Landis, C.R., T. Cleveland, and T.K. Firman, "Valence bond concepts applied to the molecular mechanics description of molecular shapes. 3. Applications to transition metal alkyls and hydrides." *J. Am. Chem. Soc.* 120:2641–2649, 1998.

[56] Loew, G. and M. Dupuis, "Structure of a model transient peroxide intermediate of peroxidases by *ab initio* methods." *J. Am. Chem. Soc.* 118:10584–10587, 1996.

[57] Loew, G. and M. Dupuis, "Characterization of a resting state model of peroxidases by *ab initio* methods: optimized geometries, electronic structures, and relative energies of the sextet, quartet, an ddoublet spin states" *J. Am. Chem. Soc.* 119:9848–9851, 1997.

[58] Mackerell, A.D., et al., "All-atom empirical potential for molecular modeling and dynamics studies of proteins" *J. Phys. Chem. B* 102:3586–3616, 1998.

[59] Maulitz, A.H., F.C. Lightstone, Y.J. Zheng, and T.C. Bruice, "Nonenzymatic and enzymatic hydrolysis of alkyl halides: A theoretical study of the S_N2 reactions of acetate and hydroxide ions with alkyl chlorides" *Proc. Natl. Acad. Sci. USA* 94:6591–6595, 1997.

[60] McMahon, B.H., J.D. Müller, C.A. Wraight, and G.U. Nienhaus "Electron transfer and protein dynamics in the photosynthetic reaction center" *Biophys. J.* 74:2567–2587, 1998.

[61] McMahon, M.T., A.C. deDios, N. Godbout, R. Salzmann, D.D. Laws, H. Le, R.H. Havlin and E. Oldfield "An experimental and quantum chemical investigation of CO binding to heme proteins and model systems: A unified approach based on ^{13}C, ^{17}O and ^{57}Fe nuclear magnetic resonance and ^{57}Fe Mössbauer and infrared spectroscopies" *J. Am. Chem. Soc.* 120:4784–4797, 1998.

[62] Melchers, B., E.W. Knapp, F. Parak, L. Cordone, A. Cupane, and M. Leone "Structural fluctuations of myoglobin from normal-modes, Mössbauer, Raman, and absorption spectroscopy" 70:2092–2099, 1996.

[63] Mercandelli, P. and A. Sironi "Ligand stereochemistry of metal clusters containing π-bonded ligands" *J. Am. Chem. Soc.* 118:11548–11554, 1996.

[64] Miehlich, B., A. Savin, H. Stoll, and H. Pruess "Results obtained with the correlation energy density functionals of Becke and Lee, Yang and Parr" *Chem. Phys. Lett.* 157:200–206, 1989.

[65] Müller, J.D. PhD thesis, TUM, Munich, Germany, 1997.

[66] Nienhaus, G.U., J. Heinzl, E. Huenges, and F. Parak "Protein crystal dynamics studied by time-resolved analysis of X-ray diffuse scattering" *Nature* 338:665–666 (1989).

[67] Nienhaus, G.U., J.D. Müller, B.H. McMahon, H. Frauenfelder "Exploring the conformational energy landscape of proteins" *Physica D* 107:297–311, 1997.

[68] Panchenko, A.R., J. Wang, G.U. Nienhaus, and P.G. Wolynes, "Analysis of ligand binding to heme proteins using a fluctuating path description" *J. Phys. Chem.* 99:9278–9282, 1995.

[69] Parak, F., E.W. Knapp, and D. Kucheida, "Protein Dynamics: Mössbauer spectroscopy on deoxymyoglobin crystals" *J. Mol. Biol* 161:177–192 (1982).

[70] Peterson, E.S., J.M. Friedman, E.Y.T. Chien, and S.G. Sligar, "Functional implications of the proximal hydrogen-bonding network in myoglobin: a resonance Raman and kinetic study of Leu89, Ser92, His97, and F-helix swap mutants" *Biochem.* 37:12301–12319, 1998.

[71] Post, F., W. Doster, G. Karvounis, and M. Settles, "Strucutral relaxation and nonexponential kinetics of CO-binding to horse myoglobin: Multiple flash-photolysis experiments" *B.J.* 64:1833–1842, (1993).

[72] Redi, M.H., B.S. Gerstman, and J.J. Hopfield "Hemoglobin-carbon monoxide binding rate. Low temperature magneto-optical detection of spin-tunneling" *Biophys. J.* 35:471–484, 1981.

[73] Richardson, D.E. "The angular overlap model as a unified bonding model for main-group and transition-metal compounds: a version suitable for undergraduate inorganic students" *J. Chem. Edu.* 70:372–380 1993.

[74] Richardson, R.S., E.A. Noyszewski, K.F. Kendrik, J.S. Leigh, and P.D. Wagner, "Myo-globin O_2 desaturation during exercise: evidence of limited O_2 transport" *J. Clin. Invest.* 96:1916–1926, 1995.

[75] Rovira, C. P. Ballone, and M. Parrinello, "A density functional study of iron-porphyrin complexes" *Chem. Phys. Lett.* 271:247–250, 1997.

[76] Rovira, C., K. Kunc, J. Hutter, P. Ballone, and M. Parrinello, "Equilibrium geometries and electronic structure of iron-porphyrin complexes: A density functional study." *J. Phys. Chem. A* 101:8914–8925, 1997.

[77] Russo, T.V., R.L. Martin, and P.J. Hay "Density functional calculations on first-row transition metals" *J. Chem. Phys.* 101:7729–7737, 1994.

[78] Schlichting, I., J. Berendzen, G.N. Phillips Jr., and R.M. Sweet "Crystal structure of photolysed carbonmonoxy-myoglobin" *Nature* 371:808–812, 1994.

[79] Sinclair, R., S. Hallam, M. Chen, B. Chance, and L. Powers, "Active site structure in cytochrome c peroxidase and myoglobin mutants: effects of altered hydrogen bonding to the proximal histidine" *Biochem.* 35:15120–15128, 1996.

[80] Smith, J.C. "Protein dynamics: comparison of simulations with inelastic neutron scattering experiments" *Quart. Rev. Biophys.* 24:227–291, 1991.

[81] Smith, M.L., J. Paul, P.I. Ohlsson, and K.G. Paul "Correlations between reduction potential, CO stretch frequency, and CO half-bandwidth in hemoproteins" *Biochem.* 23:6776–6785, 1984.

[82] Spiro, T.G., and P.M. Kozlowski, "Discordant results on FeCO deformability in heme proteins reconciled by density functional theory" *J. Am. Chem. Soc.* 120:4524–4525, 1998.

[83] Springer, B.A., S.G. Sligar, J.S. Olson, and G. Phillips, "Mechanisms of ligand recognition in myoglobin" *Chem. Rev.* 94:699–714, 1994.

[84] Steinbach, P.J., R.J. Loncharich, and B.R. Brooks, "The effects of environment and hydration on protein dynamics: a simulation study of myoglobin" *Chem. Phys.* 158:383–394, 1991.

[85] Steinbach, P.J. et al., "Ligand binding to heme proteins: Connection between dynamics and function" *Biochem.* 30:3988–4001, 1991.

[86] Straub, J.E. and M. Karplus, "Molecular dynamics study of the photodissociation of carbon monoxide from myoglobin: ligand dynamics in the first 10 ps" *Chem. Phys.* 158:221-248, 1991.

[87] Teng, T.Y. et al.,*Nat. Struct. Bio.* 1:701–705, 1994.

[88] Tokita, Y. and H. Nakatsuji, "Ground and excited states of hemoglobin CO and horseradish peroxidase CO: SAC/SAC-CI study." *J. Phys. Chem. B* 101:3281–3289, 1997.

[89] Vitkup, D., G. A. Petsko, and M. Karplus, "A comparison between molecular dynamics and X–ray results for dissociated CO in myoglobin" *Nature Struct. Biol.* 4:202–208, 1997.

[90] Vojtechovský, J., K. Chu, J. Berendzen, R.M. Sweet, and I. Schlichting, "Crystal structures of myoglobin–ligand complexes at near–atomic resolution." *Biophys. J.* in press, 1999.

[91] Wells, R.M.G., M.J. Hudson, and T. Brittain, "Function of the hemoglobin and the gas bubble in the backswimmer *anisops-assimilis* (*hemiptera, notonectidae*) *J. Comp. Physiol.* 142:515–522, 1981.

[92] Wittenburg, B.A. and J.B. Wittenberg, "Transport of oxygen in muscle" *Annu. Rev. Physiol.* 51:875–878, 1989.

[93] Woolley, R.G. "Ligand-field analysis of transition-metal complexes" *Intern. Rev. Phys. Chem.* 6:93–141 1987.

[94] Zheng, C., V. Makarov, and P.G. Wolynes "Statistical survey of transition states and conformational substates of the sperm whale myoglobin-CO reaction system." *JACS* 118:2818-2824, 1996.